Railway ballast performance

Recent advances in the understanding of geometry, distribution and degradation

Shi, Can; Fan, Zheng; Connolly, David P.; Jing, Guoqing; Markine, Valeri; Guo, Yunlong

DOI
10.1016/j.trgeo.2023.101042

Publication date
2023

Document Version
Final published version

Published in
Transportation Geotechnics

Transportation Geotechnics 41 (2023) 101042

Contents lists available at ScienceDirect

Transportation Geotechnics

journal homepage: www.elsevier.com/locate/trgeo

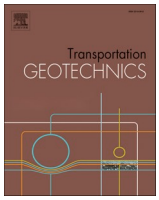

Railway ballast performance: Recent advances in the understanding of geometry, distribution and degradation

Can Shi [a], Zheng Fan [b], David P. Connolly [c], Guoqing Jing [b,*], Valeri Markine [d], Yunlong Guo [d,*]

[a] College of Civil and Transportation Engineering, Shenzhen University, Shenzhen 518060, China
[b] School of Civil Engineering, Beijing Jiaotong University, Beijing 100044, China
[c] School of Civil Engineering, University of Leeds, Leeds LS2 9JT, UK
[d] Faculty of Civil Engineering and Geosciences, Delft University of Technology, Delft 2628CN, Netherlands

ARTICLE INFO

Keywords:
Railway ballast
Ballast mechanical behaviour
Ballast particle size distribution
Railway track degradation
Ballast fouling index
Railroad dynamic performance
Parent rock
Bulk density

ABSTRACT

Railway ballast performance is dictated by a complex mix of mechanical properties. These effect its performance at the particle level for example in terms of particle degradation, but also at the track system level in terms of settlement and stability. Therefore this paper seeks to develop new understandings of ballast behaviour and identify opportunities for future research directions. First, ballast particle size and size distribution curves are discussed, considering opportunities to improve breakage, settlement and drainage characteristics. Next, particle geometry is discussed, with a focus on form, angularity and surface texture. This is followed by a discussion on the degradation mechanisms of ballast particles and the effect of fouling on permeability. Next, techniques to assess and improve ballast bulk density are discussed, such as ground penetration radar and dynamic track stabilisation. Testing methods for studying ballast are also reviewed, first considering both smaller-scale tests such as direct shear tests and the Los Angeles abrasion test. Then larger-scale laboratory testing is discussed, including large-diameter dynamic triaxial testing and the use of full-scale laboratory tracks. Finally, conclusions are drawn and suggestions for future research directions are given.

Introduction

Railway ballast is the granular material that supports sleepers on a traditional railway track. It is composed of discrete particles, typically larger than those considered in traditional geotechnical engineering. Its properties can be classified into those at the particle level and those related to the entire ballast layer. The world's railways are moving towards more sustainable operation, but also with the desire for higher train speeds and heavier freight. These aims hinge upon high performance of the track structure, the core of which is formed from ballast. However, the mechanical properties of this material are still not fully understood and as such, a variety of challenges persist:

Degradation and fouling: High contact forces and ballast layer vibration can increase the ballast wear rate, which results in an increased volume of fines within the ballast matrix. These result in more rapid ballast settlement rate particularly in wet conditions. For high-speed railways, ballast abrasion is a common degradation type, while ballast breakage is more common for heavy haul railways. In addition to increased granular fines, cohesive fines can be introduced due to mud pumping from below the ballast.

Track stability: The ballast layer accounts for up to 65% of the overall track stability on the condition that ballast layer is stabilized and compacted [1]. Stability includes three forms: 1) lateral, related to the resistance of forces in the direction perpendicular to the track, 2) longitudinal, related to the resistance of forces in the direction of train passage, 3) vertical, related to the resistance of the vertical forces induced by the train. Typically, lateral and longitudinal stability are of concern for track buckling, while vertical stability is concerned with the allowable vertical track deflection under train loading.

Damage during maintenance: Track maintenance (e.g. tamping) is commonly used to correct track geometry, however, can cause damage to the ballast particles due to the abrasion between the tamping tines and stones [2]. This results in the production of additional fines, meaning the ballast life may be shortened.

To better understand the above challenges, it is useful to make a distinction between ballast layer properties and ballast particle properties. Therefore tables Table 1 and Table 2 describe the most important properties related to both.

* Corresponding authors.
E-mail addresses: gqjing@bjtu.edu.cn (G. Jing), Yunlong.guo@tudelft.nl (Y. Guo).

https://doi.org/10.1016/j.trgeo.2023.101042
Received 8 May 2023; Received in revised form 31 May 2023; Accepted 31 May 2023
Available online 7 June 2023

Table 1
Ballast particle properties influencing ballast mechanical behaviour.

Ballast particle properties	Description	Field measurement	Lab measurement	Numerical simulation
Particle size and shape	Ballast particle size is an important concern in railway ballast standards. It determines if the crushed rocks fall within limits to be used as ballast. Particle shape is defined by three main characteristics: form, angularity and surface texture.	[3]	[4–13]	[14]
Mechanical properties	Hardness and strength, breakage and abrasion	[3]	[15–18]	[16,19–21]
Material composition	Parent rock properties include ballast material, mineral composition, weathering resistance and water resistance.	[22]	[23–25]	–
Density	Particle density relates most with bulk density and contributes to track stability.	[22,26]	[27]	[28]

Table 2
Ballast layer properties influencing ballast mechanical behaviour.

Ballast layer properties	Explanations	Field measurement	Lab measurement	Numerical simulation
Particle size distribution	Particle size distribution is also called grading, which describes the mass percentage of different size ranges retained by different sieve sizes.	[29]	[30]	[31]
Compaction	Bulk density is used to quantify the compaction of the ballast layer, which relates to particle density and particle size distribution. It contributes to track stability.	[22,26]	[27]	[28]
Fouling	Fouling is related to the build-up of small/alien particles in the ballast.	[32,33]	[34]	[35]
Permeability	This reflects the drainage ability of ballast layer.	[36]	[37,38]	[39]
Stiffness	Resistance to force in the vertical, lateral and longitudinal directions	[40–43]	[41,44]	[41]
Geometry	Ballast layer profile is the cross section of ballast layer, which includes the ballast shoulder width, shoulder height, thickness and slope.	[45]	[46]	[47]

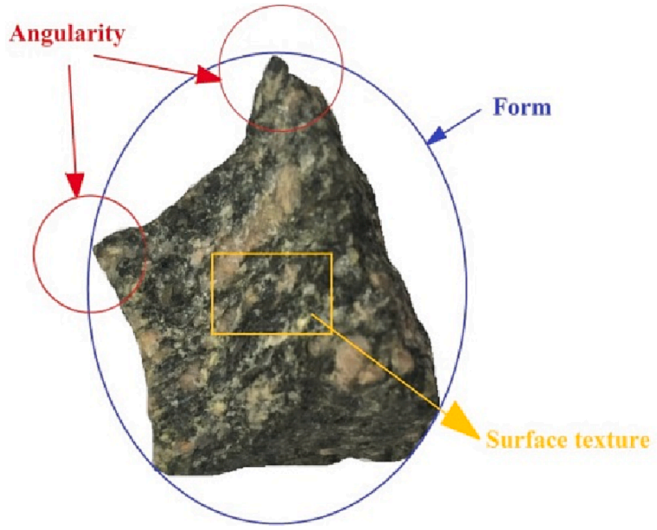

Fig. 1. *Ballast particle shape: form, angularity and surface texture (figure reproduced from [4]).*

Although these tables show a wide range of influential properties it is challenging to place weights on the influence on each regarding ballast performance because the various properties interact with each other. Further, ballast mechanical behaviour is influenced by the entire train-track-subgrade system. Considering these challenges, this paper aims to investigate them by reviewing the state-of-the-art. Firstly ballast particle size and distribution is discussed, followed by ballast particle shape. Next, degradation and fouling are discussed, followed by a section on testing methods.

Particle size and distribution

Typically the size of ballast particles varies in the range 10–60 mm. Due to the transport, handling, placement and compaction of ballast, the particle size distribution can change. Although sharp angular protrusions are the first to break, some particles may split in half or even crush into several small pieces. As the number of train cycles increases, the ballast particles deteriorate further and gradually decrease in size, but even after these changes, more than 90% of the ballast particles remain in the original range of 10–60 mm, even after several million loading cycles. This is because the majority of ballast particles are around 30 mm in size, a size that is not easily broken, while ballast particles larger than 40 mm are more easily broken [4].

Individual ballast particle size

Ballast particle size is different from ballast PSD. The ballast PSD describes the size distribution of a volume of ballast, while the ballast particle size in this section refers to the individual particle size.

Researchers have performed studies on the effect of ballast particle size on ballast mechanical behaviour, however often reached differing conclusions. Because the particle size changes during the tests, as the results of multiple types of ballast particle degradation. In addition the ballast shape also contribute to the ballast particle degradation. For example, the elongated and flaky particles, as well as bigger size particles are more prone to breaking [4], e.g., splitting into two pieces or more pieces. Two aspects are discussed in this section: 1) how ballast particle size influences ballast mechanical behaviour and, 2) how ballast particle size is linked with other ballast properties.

Firstly, the shear strength of ballast particles increases with increasing particle size. Because large particles have higher mass and thus higher inertia. For this, the contact forces between large particles are higher, which provides higher interlock between particles. This increases the inter-particle friction, and thus increasing the ballast assembly stability [5,6]. However, this theory is proved as solid only when the ballast particles were assumed to be non-crushable, in other words, very low rate of breakage happened [7]. Small ballast particles can lead to higher compaction, which makes the ballast layer higher stiffness and stable shear strength. Therefore, there is still no certain conclusion on this.

Secondly, particle size is closely influenced by the other conditions in all kinds of tests, such as the scale effects (also considered as boundary conditions) and particle morphology. On one hand, test container size for ballast should be more than 6 times larger than the biggest ballast particle (circa 60 mm). A summary of configurations for ballast test rigs

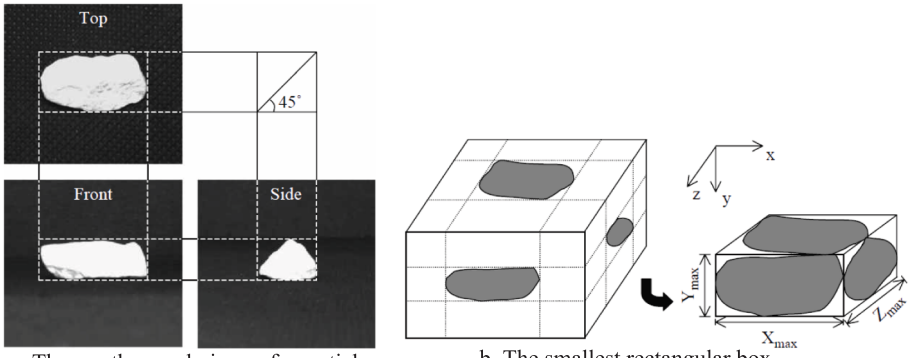

a. Three orthogonal views of a particle b. The smallest rectangular box

Fig. 2. *Three dimensions of one ballast particle (figure reproduced from [9]).*

and container sizes can be found in [8]. This leads to the interaction between ballast particles and the boundary affects ballast movement, resulting in unpredictable test results [48]. On the other hand, larger particles have increased angularity and rougher surfaces (e.g. Fig. 1), which results in increased particle interlocking.

Lastly, in most earlier studies, there is no clear distinction between the ballast particle size and the ballast particle size distribution. Particle size distribution is the mostly used method to quantify ballast particle size. Because measuring each particle size in one ballast sample is difficult, furthermore, ballast particles have multiple dimensions as shown in Fig. 2, which means each dimension size can be seen as particle size. Obtaining PSD by sieving is the most efficient way.

Considering these complex conditions, the mechanical behaviour of the ballast and ballast layer are challenging to predict. This is mostly because the ballast is inhomogeneous and effected by a wide range of properties.

Particle size distribution of a ballast volume

The particle size distribution of railway ballast has a significant influence on the track's mechanical behaviour. The ballast standard [49] (code: TBT2140-2008) specifies that the ballast particle sizes should be within grade 22.4–63 mm (sieve size). Standards used in other countries also require ballast sizes in the range of 20–60 mm (roughly the same) [50,51], and most of the particle sizes are in the range of 20–40 mm. A comparison of ballast PSDs in different international ballast standards is shown in Fig. 3. Ballast particle size has an influence on ballast layer mechanical behaviour, such as deformation, strength, elastic modulus, and it dictates the PSD.

Compared to traditional geotechnical materials, ballast particles are bigger and have high angularities. There is no viscous forces between two ballast particles [52] and because of these properties, PSD is crucial for ballast mechanical behaviour. The shear strength, deformation resistance and drainage of ballast layers are greatly influenced by the PSD of the ballast particles. The ballast layer mechanical behaviour is mostly dictated by the contact forces between ballast particles. This is important because PSD can change the compaction level and the contact numbers, then influencing the contact forces.

For different types of PSD, there is a rough classification, dividing them into two types: narrow PSD and wide PSD. Wide PSD ballast layers offer higher strength and deformation resistance compared to narrow graded PSD ballast layers, because the lower layer porosity and more compacted ballast can restrict particle rearrangement (particle movements) [10,53].

However, under the condition of high ballast layer moisture, the wide PSD ballast layers have lower loading capacity and are less permeable. Moisture affects ballast layer performance, especially when fine particle fouling (e.g., soil) is involved. Note that sand fouling might increase the bearing capacity of ballast layer, which makes the wide PSD ballast layer has wider PSD. In addition, wide PSD ballast particles are not easily handled at ballast transportation and ballast layer construction, because the ballast particles have a greater chance to separate into different layers. In other words, small ballast particles shake down to the bottom layer, while larger ballast particles stay upper layer. In contrast, narrow PSD ballast layers have enough voids to provide good drainage. In addition, narrow PSD ballast particles are easy to transport and are good for new ballast layer construction, because they are not easy to separate into layers. However, the narrow PSD ballast particles also have disadvantages. The biggest concern is ballast breakage, which is more prone to happen compared to wider PSD ballast particles. Because the coordination number of each ballast particle (narrow PSD ballast particles) is smaller than that of wide PSD ballast particles, which leads to stress concentration [4,54].

PSD can be classified into: uniform PSD, medium uniform PSD and intermittent PSD. Uniform PSD means that the particles are almost the same in each size range. Intermittent PSD means that the particles are in two size ranges: one is big (e.g. 40–50 mm) and the other is small (e.g. 15–25 mm). Under cyclic loading, the uniformity of PSD has a significant effect on the axial and volumetric strains of ballast assembly. Results show that uniform PSD ballast particles produce high axial and volumetric strains when the initial compaction of the ballast particles is not sufficient. Medium uniform PSD and intermittent PSD ballast particles are denser and have high coordination numbers of each ballast particle. Coordination number is the number of contacts on one ballast particle to its neighbouring particles. Therefore, medium uniform PSD and intermit PSD can improve the shear strength of ballast particles and reduce the ballast layer deformation [30,55]. However, narrow PSD is preferred for ballast layer maintenance, because it is more straightforward to tamp using tamping machines and remove fines [56].

PSD uniformity can be defined using the coefficient of uniformity ($C_u = d_{60}/d_{10}$). In most cases, the coefficient of uniformity ranges from 1.5 to 3.0 with an average value approximately 2. Even small changes in the coefficient of uniformity can affect the deformation and crushing properties of the ballast particles. However, until now no clear explains have been given about why this kind of PSD is better than others.

The relationship between the C_u of ballast particles and particle breakage was studied in [57]. Results show that the particle breakage decreases as C_u increases. The hypothesis is that intermittent PSD ballast particles (high C_u value) do not include ballast particles that are prone to crushing. In addition, the particles have more contacts with neighbouring particles [51]. Therefore, the intermittent PSD ballast particles have less breakage than the uniform PSD ballast particles.

In laboratory tests (e.g. direct shear test), a slightly wider PSD is used because it can reduce ballast layer deformation and drainage is usually ignored. A coefficient of uniformity greater than 2.2 reduces ballast breakage. Regarding drainage, a coefficient of uniformity of 2.2 provides sufficient drainage as long as the ballast layer is not heavily fouled and a drainage system is built along the track.

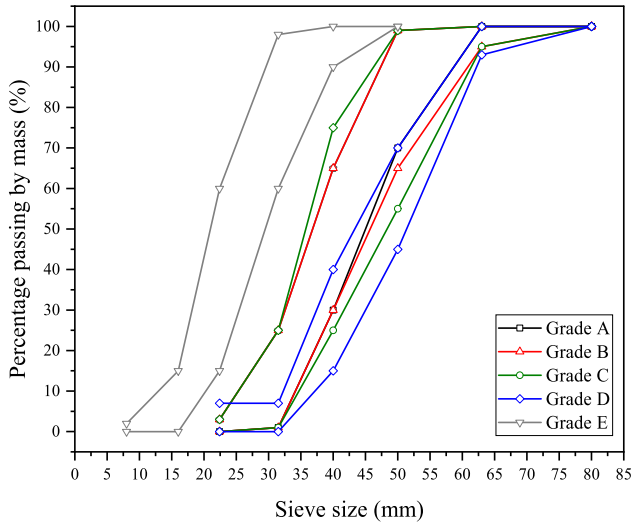

(a) British standard (EN933-1)

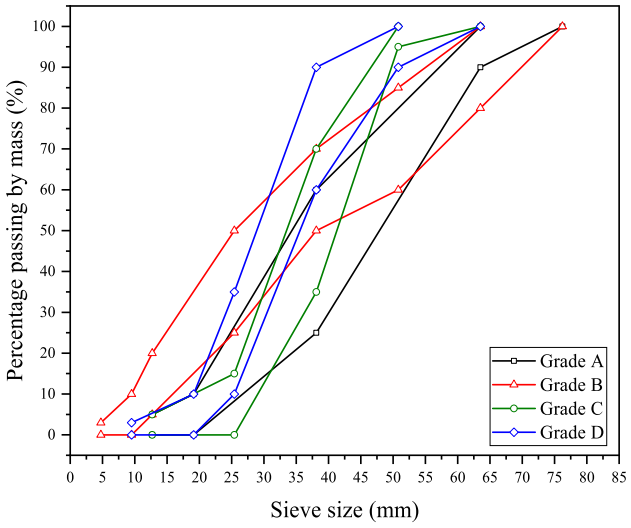

(b) American standard (ASTM-C136)

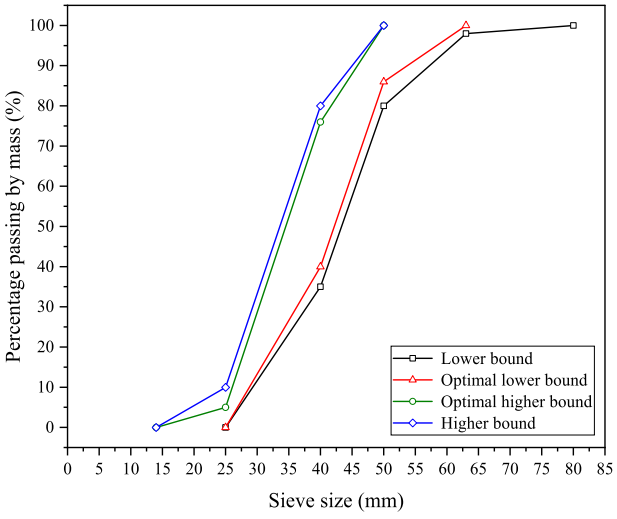

(c) French standard (NF EN 13450)

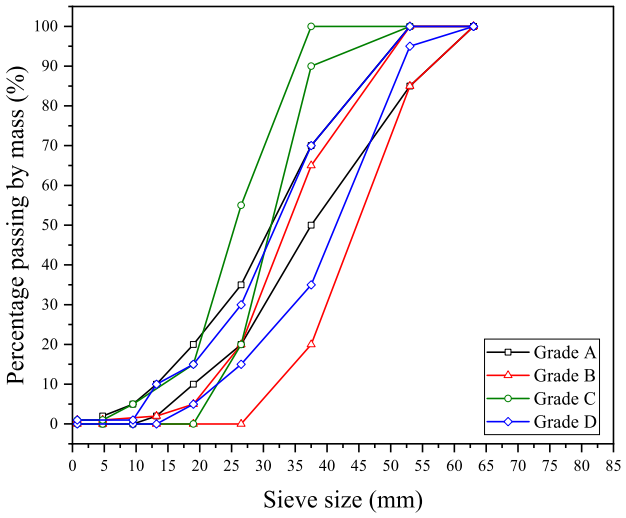

(d) Australian standard (AS 1141.11.1)

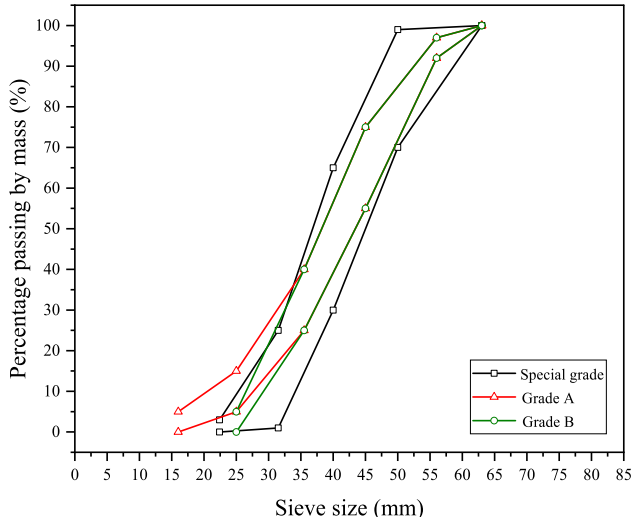

(e) Chinese standard (TB/T2140-2008)

Fig. 3. Particle size distributions in different ballast standards, the Grade A-E refer to different requirement of PSDs for different conditions, such as line class.

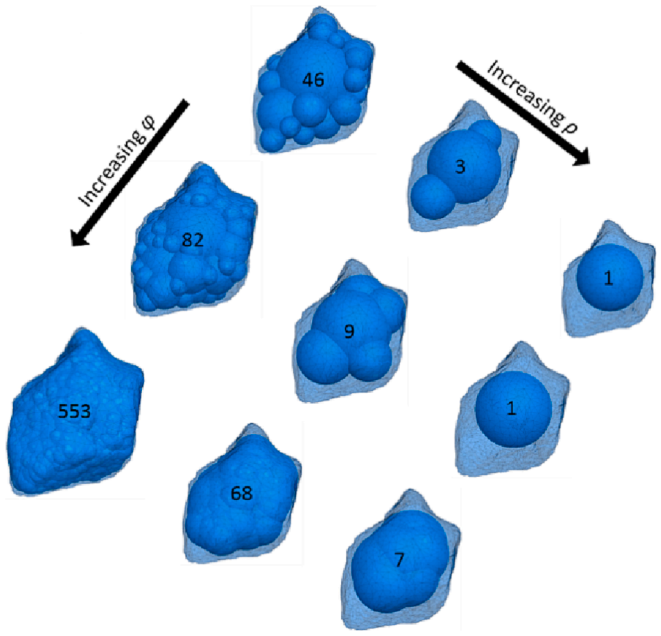

Fig. 4. *Sphere or spheres for representing one ballast particle (figure reproduced from [62]).*

The medium coefficient of uniformity is recommended [17,18]. However, in [57], an optimum PSD (with $1.8 \leq Cu \leq 2.0$) is recommended for high frequency cyclic loading, which means deciding the coefficient of uniformity should also consider the loading type (e.g. high-speed railway vs freight).

Other studies show the same or similar results related to the coefficient of uniformity. For example, in [58], the conclusions are given: (1) Widening the PSD increases the shear strength of the ballast particles, (2) the shear strength of the ballast particles depends not only on the value of the coefficient of uniformity but also on the average size of the ballast particles (d_{50}), (3) increasing the average ballast size (d_{50}) increases the shear strength of the ballast.

Numerical simulations using DEM models are an alternative way to study PSD influence on ballast layer mechanical behaviour. DEM models simulate ballast particles as discrete elements, and are attractive because the ballast properties are easy to control. Even so, the results are still complex and like lab testing, the results inconclusive. For example, in [31], four PSDs were studied by comparing their shear strength. Two of them were upper and lower bands of the American PSD specification (AREMA #4), while the other two are another upper and lower bands of the American PSD specification (AREMA #24). Results showed the two AREMA #4 PSDs had different shear strengths, while the other two didn't. This was caused by the particle arrangement of the compacted ballast, which is also difficult to control in DEM simulations. Another common reason for DEM simulation results diverging from lab test results is that the ballast particles are approximated as spheres. For example, in Fig. 4 two parameters determine the sphere number (shown on each particle). ρ is the diameter ratio of the smallest to the largest spheres and ϕ is the maximum sphere-sphere intersection angle (see [59]). More studies on PSD using DEM can be found in [60,61].

Particle shape

Attempts have been made to characterise the ballast particle shape however due to the complexity and irregularity of particle shapes, no universally recognised parameters for particle shape characteristics have been established. For example, although various shape characteristics (i.e. flakiness, elongation, sphericity, angularity and surface structure) have been proposed [62,63], only the flakiness and elongation parameters are commonly mentioned in international ballast standards.

Studies have been performed to investigate how ballast particle shape influences ballast mechanical behaviour using laboratory tests and DEM modelling. For example, in [64], form, angle and surface texture (Fig. 1) are shown to be the key factors affecting ballast performance. They influence the interlocking of ballast particles, thus have a large impact on ballast strength and ballast layer deformation. Ballast layer deformation can be caused by particle movement and rearrangement, ballast breakage and abrasion, which are influenced by the ballast particle shapes.

However, the ballast particles have large inhomogeneity. Although in this study the authors controlled the variables, the cohesion and friction angle yielded different values. For example, the friction angle of ballast is in the range of 45-65°, which is not a very small range [17,65,66]. The possible reason for this is the ballast particle shapes are very difficult to control. For example, the form, angularity and surface texture of ballast particles make a major contribution to the slip resistance and particle breakage of ballast [12]. The angularity and texture are the main influencing factors on the slip resistance of ballast particles. Surface texture is a major factor influencing surface friction because rough surface particles have a greater frictional force than smooth surface particles.

Other studies using DEM have shown particle shape has a significant effect on the mechanical behaviour of ballast layers, as shown in Fig. 5. For example, the effect of particle angularity and sphericity on ballast behaviour has been studied in depth. These studies concluded that ballast particles with sharp angularities and rough surfaces significantly increased interlocking between ballast particles, providing increased mechanical behaviour [67]. In addition, studies have also simulated diverse laboratory geotechnical tests, such as the angle of repose test and direct shear test. For example, using DEM direct shear test models, [68] considered the shear strength of ballast particles with different elongations. Different shapes of ballast can be produce with different angles of repose [68]. Using the DEM direct shear test models, the sphericity of the particles and their effects on the overall shear strength of the ballast particles [69]. In a recent study [70], the effect of ballast particle shapes on the repose angle of the ballast particles was studied, as shown in Fig. 5d&e.

Form

A straightforward way of describing 'form', is to use the longest (L), shortest (S) and intermediate (I) orthogonal dimensions of a ballast particle (Fig. 2), and combine two or all of them into an indicator [13,63]. These indicators mainly describe the form as flaky, elongated and cubic. The nouns of these shape characteristics are flakiness, elongation and cuboidal-ness.

Ballast standards in different countries use different values for classifying form. For example, in [72], I/L is the elongation and I/S is the flakiness. These values are calculated for each ballast particle in the sample, and their percentages determines whether the sample consists mainly of flat, elongated, flat and elongated or cubic particles. In the Chinese ballast standard [49], the requirement is that elongated or flaky particles cannot be over 20%. The British standard [50] considers a particle to be flaky if the ratio of I/S is greater than 1:1.67. The American standard proposed three ratios: 1:2, 1:3 and 1:5, and one of them can be used. The Brazilian standard uses the ratio 1:2. The definition of elongated particles varies from standard to standard. The British standard defines elongated particles as that the I/L is greater than 1:1.8, while the American standard and the Brazilian standard use the same ratio [72]. If the particle is not elongated or flaky, then it is seen as a cubic particle.

Flaky and elongated particles are easy to break, which has great impact on the ballast layer behaviour due to sudden ballast-ballast contact force changes. For example, in [73], the results of uniaxial static load tests on ballast particles showed that the most broken/

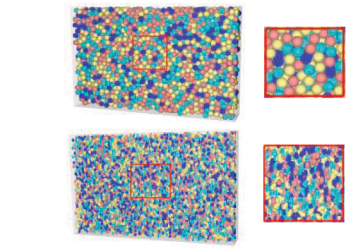

a. Particles are spheres or polyhedron

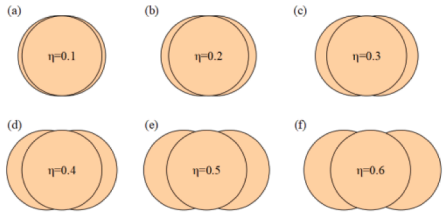

b. Particles are 2D multi-spheres to present particle elongation

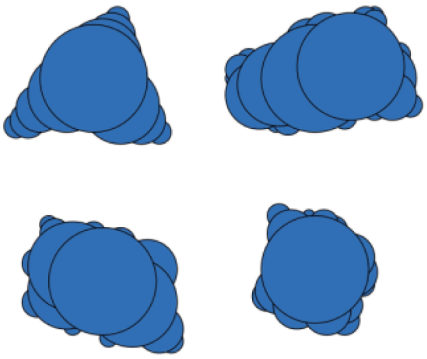

c. 2D multi-sphere particles (clumps)

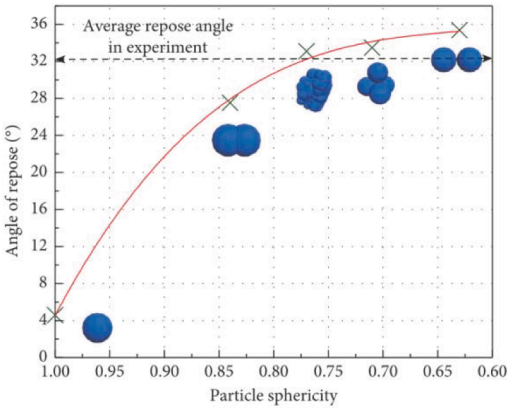

d. Effects of particle sphericity on the angle of repose (figure reproduced from [70])

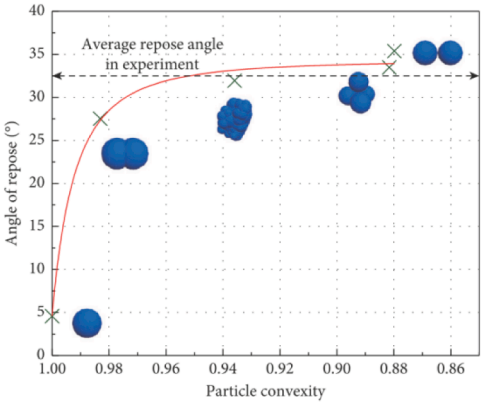

e. Effect of particle convexity on the angle of repose (figure reproduced from [70])

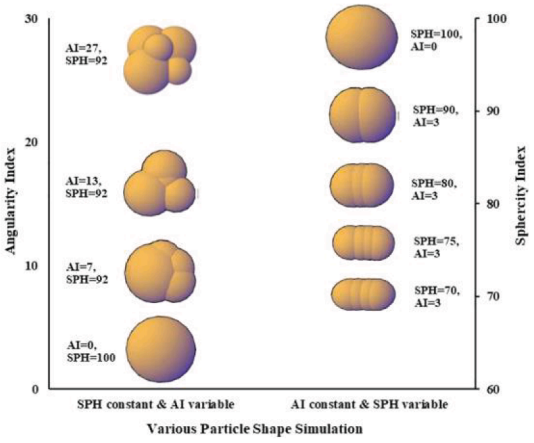

f. Different particles with diverse AI and SPH values (figure reproduced from [71])

Fig. 5. Comparison of DEM models with different ballast particle shapes (angularity and form).

degraded particles are flaky ones, while the least broken particles are cubic ones. Another example in [4] concluded from Los Angele abrasion (LAA) tests and image analysis that higher LAA losses could be observed for flaky and elongated particles than for cubic particles.

Without breakage, flaky and elongated ballast particles (also named as non-cubic particles) can provide same or improved ballast layer behaviour, for example higher shear strength [74]. However, the rapid degradation of the non-cubic particles (Fig. 6) causes the ballast layer behaviour to be unpredictable. For example, non-cubic particle breakage changes the PSD of the ballast layer, which leads to differential settlement. In addition, the breakage of large non-cubic particles in the middle can produce two pieces of cubic particles, and each of them has at least one fresh rough surface. This can increase the ballast layer shear strength. However, if one of the two pieces is small, the degradation type is not breakage, but angularity loss, which may reduce the ballast layer shear strength.

Ballast particle shape influences the sieving results of particle sizes. Because ballast particles have irregular shapes in 3 dimensions they can match multiple sieve sizes. For example, in [13] image analysis was used to quantify the shapes and sizes of ballast particles between 9.5 mm and 62.5 mm. Results show that the larger ballast particle sizes have less ratio regarding shortest/longest dimensions (S/L), as shown in Fig. 7. This means the larger size ballast particles tends to be more elongated or flaky, which is deviating from spherical. In addition, the larger size ballast particles have high angularity. In [75,76] and [77], similar conclusions were obtained, which is larger size ballast particles usually have a lower elipsoidness (higher angularity) compared to smaller ballast particles, as shown in Fig. 7.

Sphericity defines the roundness of ballast particles, which is another way to reflect if the ballast particle is cubic which can contribute most to ballast strength [52,78]. Because the shape is relatively difficult to crush, it serves well as a ballast layer skeleton. Some dimensions of

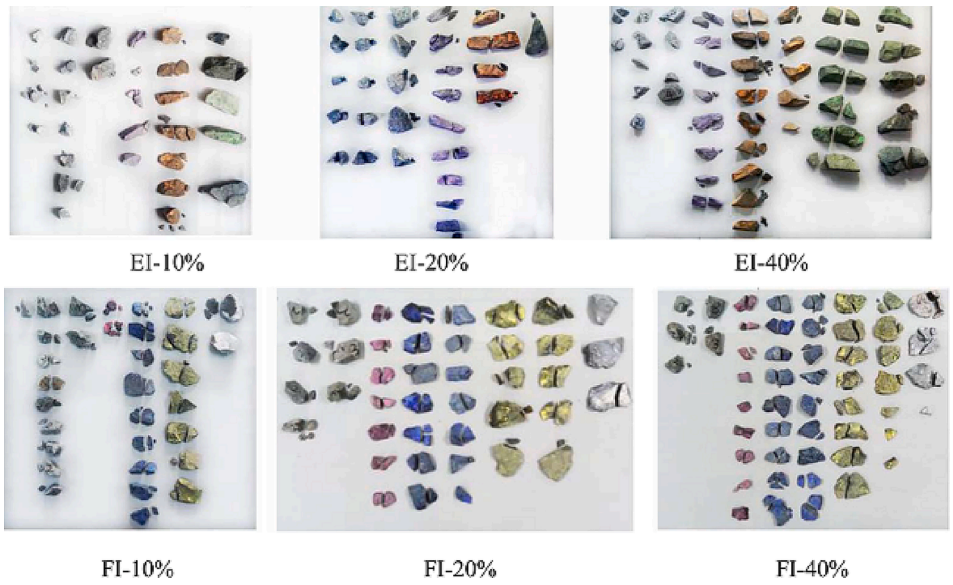

Fig. 6. *Non-cubic ballast particle breakage after direct shear test (figure reproduced from [74]).*

elongated and flaky particles are larger than others, which may crush easily, causing sudden ballast layer failure. The spherical particles are stronger under load than flaky or elongated particles, but they may have low slip resistance due to their propensity to roll. Therefore, cubic particles are a suitable shape, a finding which was also demonstrated in [79], as shown in Fig. 8.

Spherical ballast particles indicate that the ballast particles have lost their angularities. Studies [67,69,80] showed that ballast particle angles can increase the interlock between ballast particles, which in turn increases the shear strength of the ballast particles, as shown in Fig. 9. Angular ballast particles have a larger inter-particle friction angle compared to spherical ballast particles. With the increase in particle angles, ballast particle movement is restricted (by surrounding particles), thus increasing the shear strength of the ballast particles.

The shapes of ballast particles, especially the sphericity and angularity, dictate the contact stresses between ballast particles. As shown in Fig. 10, when the contact area between two particles increases, the friction between the two particles increases, thus increasing the particle interlock. Two studies focused on the ballast-ballast contact [82,83], show that the friction coefficient changes with the normal contact force with a very large range from 0.2 to 1.0. These studies used contact force as the variables, but not the contact stress meaning DEM simulations can develop more on this part - for example, friction coefficient changes with contact stress (Fig. 10).

In [17], a different conclusion was obtained. Results showed that the friction angle of ballast particles is not significantly related to the ballast particle abrasion degree, as shown in Fig. 11. In the figure, R is the linear regression coefficient; C is the ballast cohesion; K is the revolution number.

Specifically, the granite ballast particles were subjected to the abrasion machine with different number of machine revolutions. Then, triaxial tests were performed on the worn ballast particles. It was found that the stress deviation value of the maximum deflection stress decreased. In addition, the cohesive force of the ballast particles decreased, while the friction angle did not decrease to a significant extent. This means that as the ballast particle gradually approaches a spherical shape, the cohesive force drops to zero, which leads to a reduction in the shear strength of the ballast particles. Because of this, in Canada, strict control of the ballast surface roughness is therefore used, rather than direct control of the ballast particle shape [84]. These conclusions result from tests where ballast particle shapes are hard to quantify. In addition, only classifying particle shape into form, angularity and surface texture overlooks several important properties when correlating the particle shape with the ballast layer behaviour. Further, worn ballast can be more easily compacted, which compensates for low ballast-ballast contact friction.

Another study concerning the sphericity of ballast particles was performed in [85]. This study shows that freshly crushed ballast particles have higher Roundness Index values compared to natural cobbles and recycled ballast. The freshly crushed ballast particles provide higher inter-particle friction angle, which is consistent with the conclusions obtained in [7]. This study shows that Roundness Index may be suitable to present ballast shape when correlating the shape with ballast behaviour, as shown in Fig. 12.

Angularity

The angularity of ballast particles influences compaction because angularity can change the shakedown behaviour. In addition, the sharp angularity of ballast particles is easy to lose during service life. Angularity has a clear relationship with the particle sphericity, because once ballast particle losses all its angularity it becomes spherical.

In [86], results show that particle angularity and PSD directly influence the porosity under the same compression force. Ballast particles with higher angularity produce higher porosity. This also explains the experimental results in [87], that rounded ballast particles produce more settlement, because without angularities the ballast particles can move more easily relative to each other. In other words, the angularities around one ballast particle lock up this ballast particle. Without these interlocks, rounded ballast particles are more prone to rearrange. This is consistent with the conclusion presented in [7] that ballast angles increase the frictional interlocking between ballast, thereby increasing the shear strength of the ballast layer.

Ballast particle angularity loss is also influenced by particle form. In [4], compared to cubic ballast particles, flaky and elongated ballast particles have greater volume loss and are more prone to losing their sharp angularities. This also results from the fact that flaky and elongated ballast particles have sharper angularities.

In [88,89], DEM modelling was used to show that ballast particle angularity influences ballasted track stability (lateral resistance from ballast to sleeper), as shown in Fig. 13. To be more specific, ballast particles with high Angularity Index (AI) and low non-cubic shapes (F&E, flat and elongated ratio, represents particle form) provide high lateral resistance from ballast to sleeper. In this DEM modelling, ballast

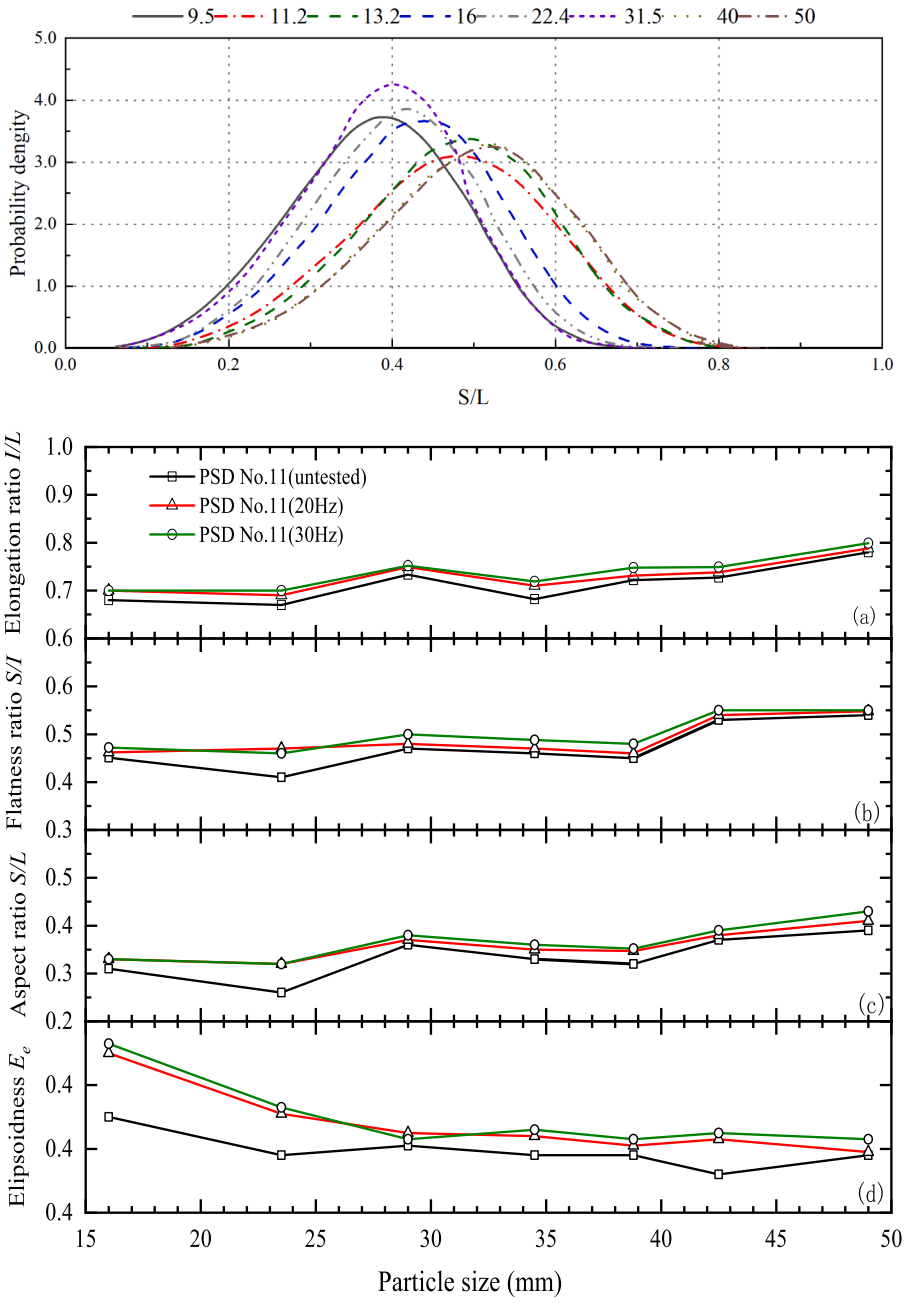

Fig. 7. *Ballast particle shape and size interaction demonstration (figure modified after [13,76]).*

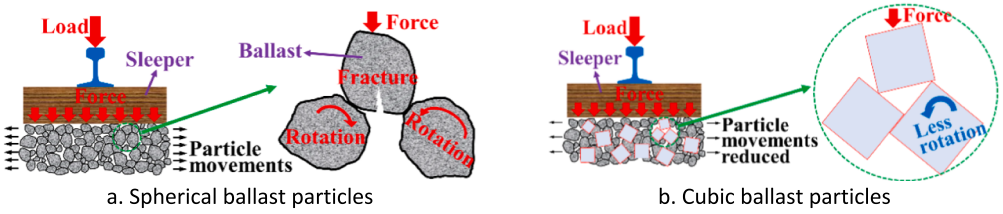

Fig. 8. Comparison of different ballast particle shape on slip resistance.

particle breakage and abrasion were not considered, which means that ballast particle degradation during the tamping was not simulated in the DEM model. However, in most cases, the angularities of ballast particles (also the AI) reduce during the tamping, and the non-cubic particles are more prone to crushing.

In [80], similar DEM modelling was performed but with direct shear test models to test the influence of Angularity Index on the shear strength of ballast particles. Note that the particles in the DEM modelling are non-crushable. In addition, the rotation of ballast particles with different AI values were also compared. The results show that high AI

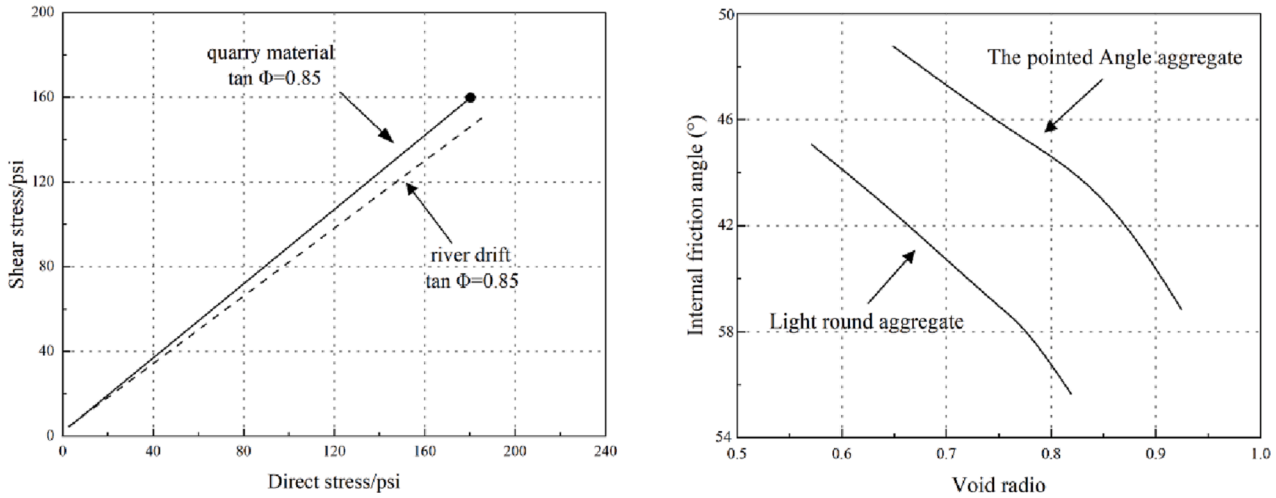

Fig. 9. *Ballast particle shape effects on shear strength and inter-particle friction angle (figure modified after [81]).*

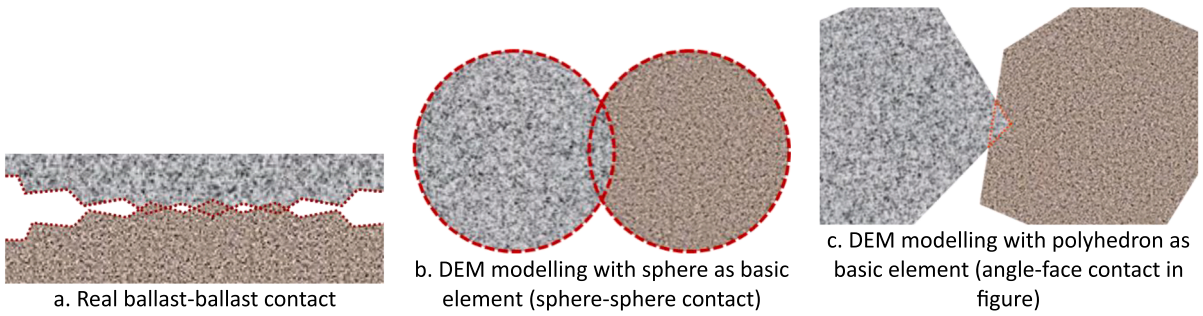

Fig. 10. Contacts between ballast particles in reality and DEM modelling.

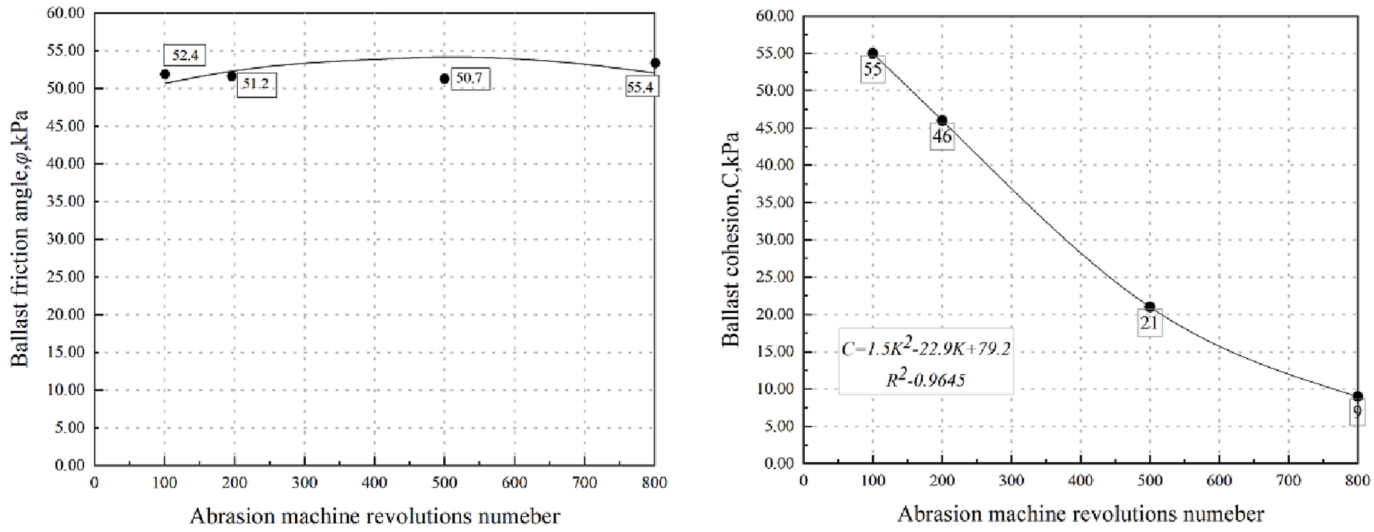

Fig. 11. *Shear strength and friction angle of ballast with different shapes (figure reproduced from [17]).*

ballast particles make the skeleton stronger (made by larger particles) thus providing better resistance to failure and deformation.

Surface texture

Most ballast standards specify that crushed rocks must have at least three fresh surface with high roughness. For example, the Chinese ballast standard [49] strictly requires that all ballast particle surfaces must be new fresh ones. These specifications aim to ensure a minimum surface roughness of each ballast particle, because it is assumed that fresh fracture surfaces have higher roughness compared to old surfaces. The old surfaces have been made smooth through mechanical wear and weathering.

The roughness of ballast particles has both positive and negative effects on ballast layer behaviour.

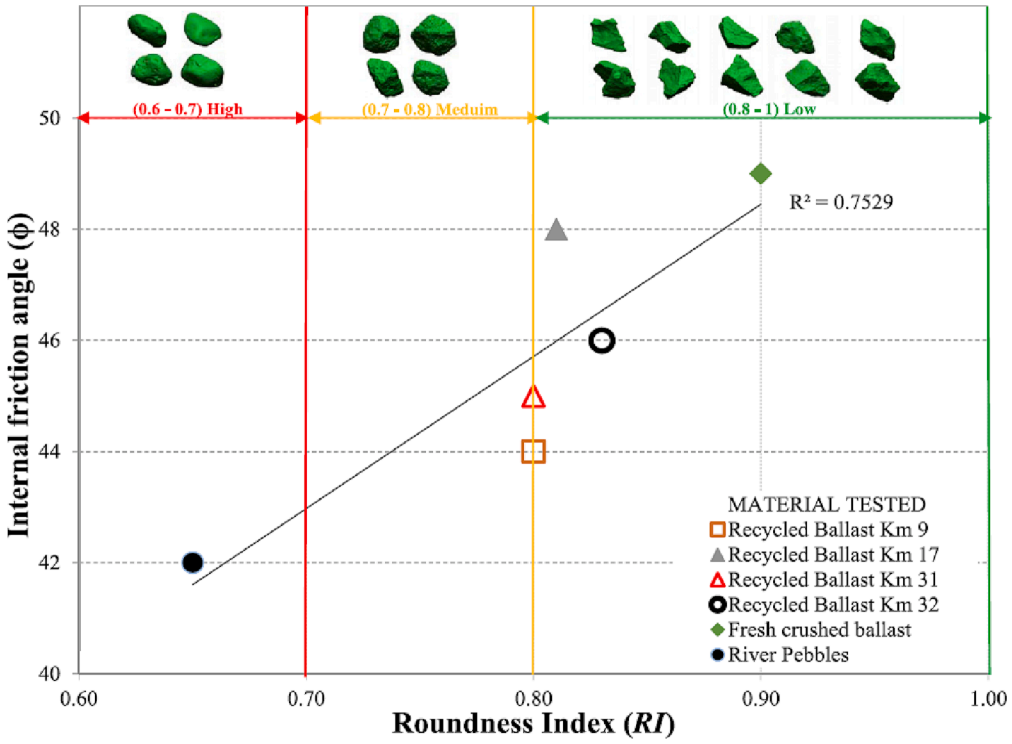

Fig. 12. *Relationship between inter-particle friction angle and Roundness Index () reproduced from* [85]*).*

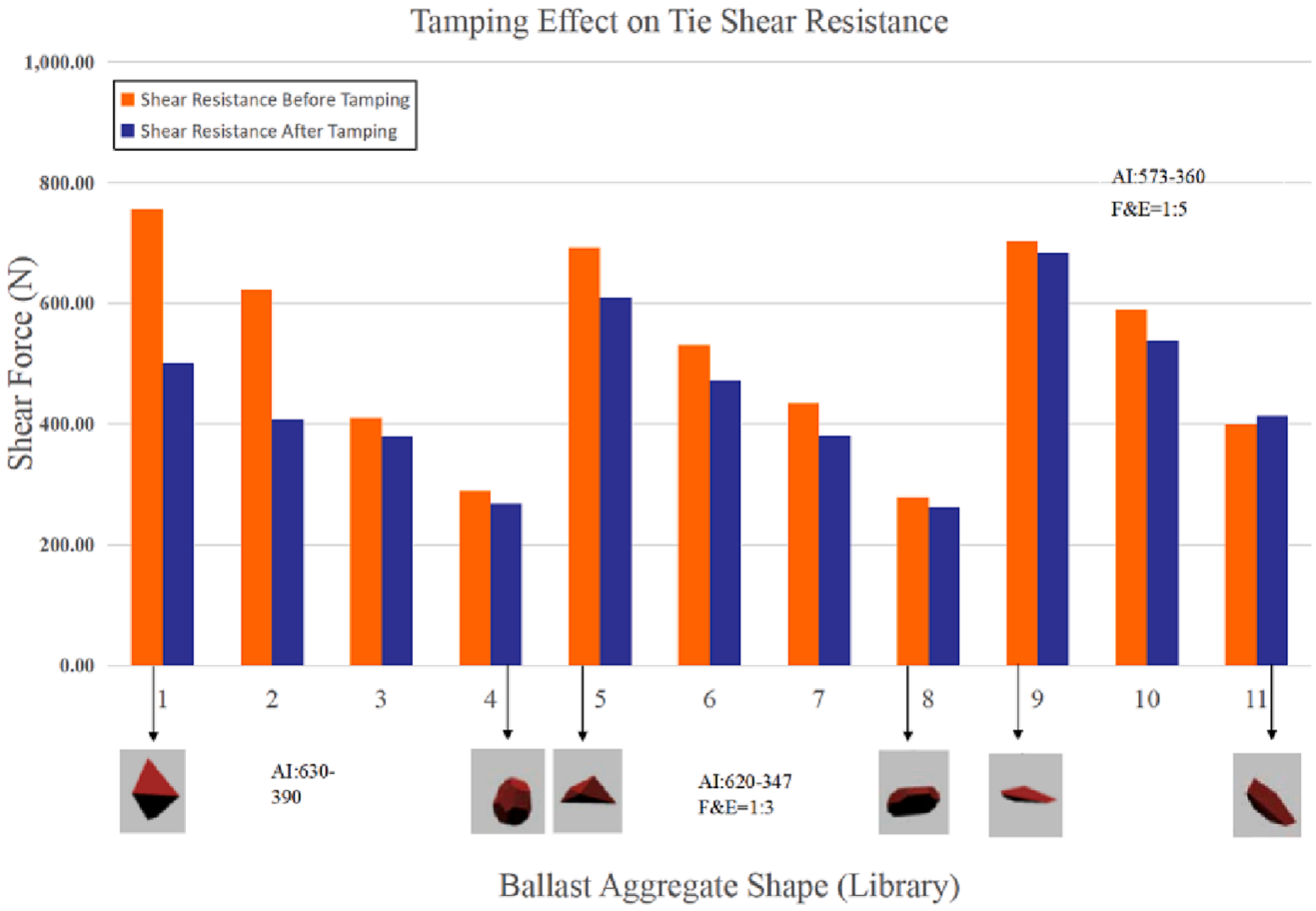

Fig. 13. *Shear forces (lateral resistance) of ballast particles with different angularity index and forms (figure modified after* [88]*).*

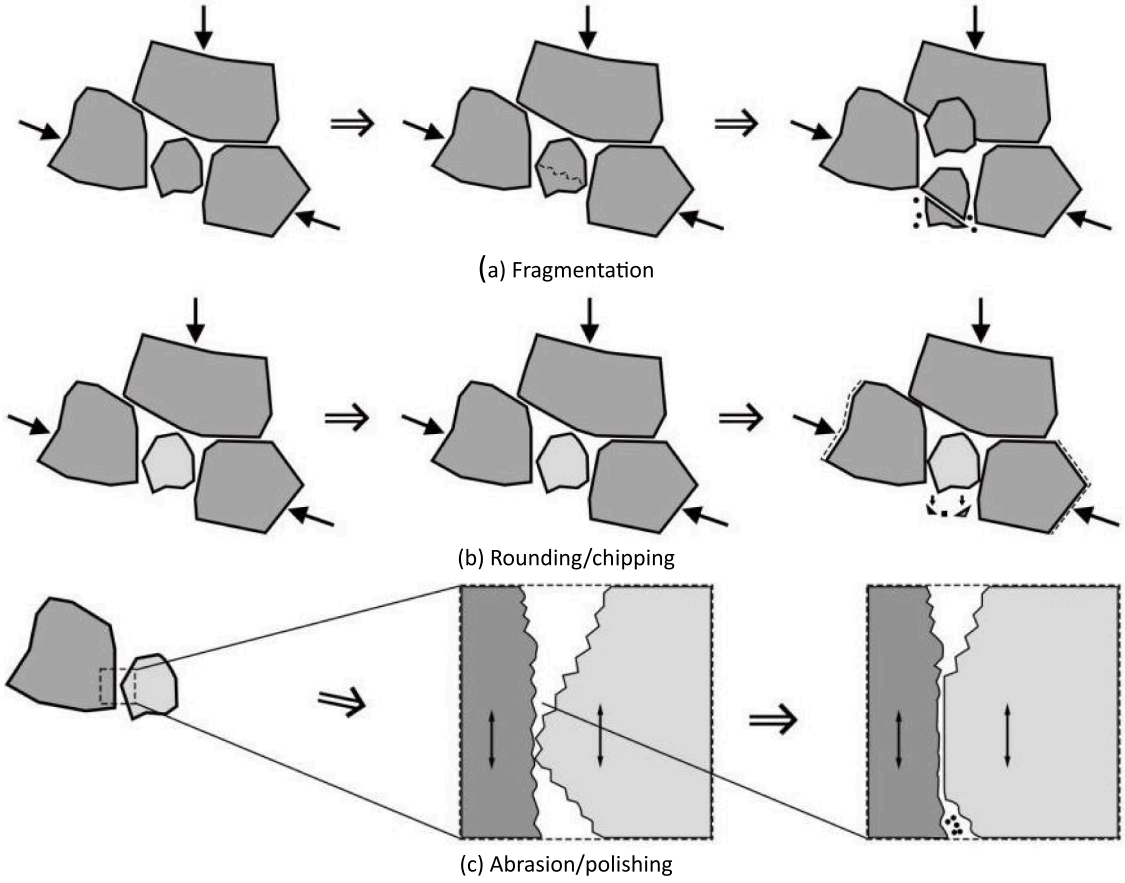

Fig. 14. Three types of ballast particle degradation.

- Positive effects. A rough particle surface is important for creating high inter-particle friction, which improves shear strength and ballast layer stability (less settlement, high resistance to sleeper) [84,90,91]. Ballast particle surface texture also influences ballast layer compaction, but it has little influence on PSD.
- Negative effects. Ballast particles with high surface roughness have a higher chance of particle degradation due to the small ballast-ballast contact area, which leads to high contact stresses and sudden failure.

The parent rock of ballast particles also influences ballast particle surface roughness. In [92], impact loading tests were carried out on ballast particles made by three types of crushed rock materials: basalt, marl and trachyte. The impact loading was applied by a large-scale impact loading setup. The test results showed that for the same PSD and impact loading, the basalt parent rock had a stronger point load strength, but its surface roughness and angularity were the most significantly reduced. This means the basalt ballast particles were the most damaged. This may result from the fact that the crushed basalt ballast has a greater surface roughness [93].

Particle shape quantification

Due to the complexity and irregularity of particle shapes, no universally-accepted means for particle shape characteristics have been established. The various shape characteristics (i.e. flakiness, elongation, sphericity, angularity and surface roughness) are still not enough to correlate the ballast particle shapes with ballast layer mechanical behaviour. Because these shape characteristics are mostly still in 2D, this means they cannot describe the particle on a 3D level. It is very important to propose parameter to characterise the sharp edges of one ballast particle, which is usually rapidly worn during the relative motion between two contacted ballast particles. The edge-surface and edge-edge contacts between ballast particles also contribute greatly to the particle interlocks.

In ballast standards (e.g. [49,50]), shape evaluation for individual ballast particles is limited. Only elongated and flaky shape particles are distinguished, which are also named as non-cubic particles. The standards require the mass proportion of non-cubic ballast does not exceed a certain value. However, this method is crude and typically ballast layer construction in the field does not strictly obey such a requirement. More importantly, there is a research gap regarding the accurate evaluation of ballast particle shape and relating the shape to the overall service performance of the ballast layer. In most cases, laboratory tests have been used instead, because field tests are time-consuming and expensive.

As the smallest scale in particle shape, it is the most difficult property to quantify, because the high-precise devices (e.g. laser scanning) have to be used, which is time intensive to check the small differences in surface texture.

In order to quantify ballast particle surface texture, a visual assessment of particle surface roughness was proposed in [58]. Particle surface roughness is visually classified into four categories. They are rough, medium rough, medium smooth and smooth. To visually estimate the particle surface roughness of ballasted samples, an index called the sample average roughness index (ARI) is used. The sample average roughness index is defined using a weighted average of roughness index:

$$ARI = \frac{\sum (W_i I_{ai})}{W_t} \tag{1}$$

In Eq. (1), W_t is the total dry weight of all the ballast samples (i in total); W_i is the total dry weight of the i^{th} ballast sample; I_{ai} is the visual roughness index of the i^{th} ballast sample. The recommended values for the average roughness index (RI) are 1.0, 0.75, 0.5 and 0.25 for the

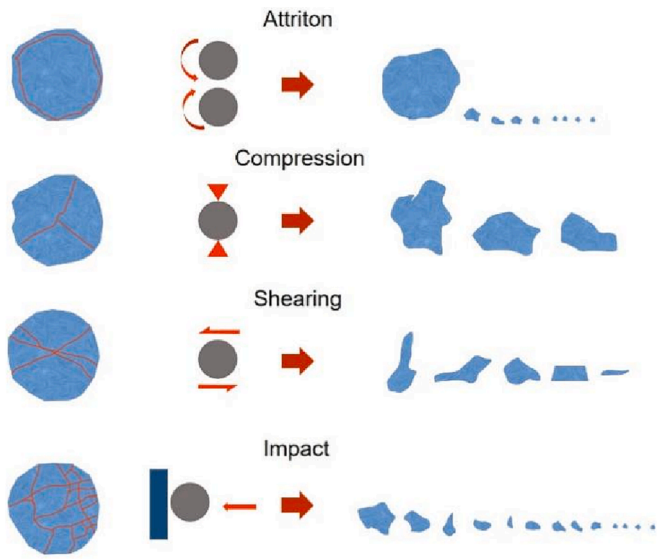

Fig. 15. Examples of ballast particle degradation types influenced by forces.

rough, medium rough, medium smooth and smooth of ballast samples, respectively.

Ballast particle shape has indices to reflect its properties, such as sphericity index, angularity index, roundness, roughness and surface texture index. These indices are calculated using volume, three dimensions, perimeter of projection, etc., which can be obtained by image analysis, as explained in [63]. Without these kinds of tools, it is very difficult to accurately quantify ballast shape due to its irregular shape. In the field, even the basic PSD of a ballast layer cannot be rapidly and non-destructively measured, because the tools usually take a long time. Therefore, it is necessary to develop a method that can rapidly measure ballast size and shape, to ultimately predict ballast layer performance.

Particle degradation and fouling

Cyclic train loading is transferred from the rail to the sleeper, and then into the ballast layer. Under cyclic loading, individual ballast particles may fracture or wear, resulting in a significant reduction in the internal friction of the ballast layer. This ballast particle degradation produces fines and small particles which affect ballast layer drainage, and potentially mud-pumping. The mixture of fines and water reduce the friction between ballast particles, thus affecting the mechanical performance of ballasted track. This ultimately leads to poor track stability and safety issues.

Ballast particle degradation

Important geotechnical properties of railway ballast, include stress–strain behaviour, particle strength, volume changes and development of pore pressures, as well as changes in permeability. These depend on the integrity of the ballast particles or the amount of particle breakage that occurs as a result of stress changes. Ballast particles subjected to stresses above the normal geotechnical range exhibit considerable particle breakage, for example due to the loading from heavy haul [94]. However, some researchers have noted that particle breakage can even occur at low confining pressures [20] and the importance of particle degradation on mechanical behaviour has been recognised. Various methods of quantifying particle breakage, factors affecting particle breakage and the effect of particle breakage on the deformation behaviour of ballast are discussed in this section.

Cyclic loading can put pressure on the ballast layer, especially ballast under the sleeper (below the rail), where the stresses are greatest [95,96]. This stress can lead to ballast particle breakage, of which there are two types. The first type is corner breakage, where the sharp edge becomes rounded. The second type is particle splitting fracture (for example, in the middle, into 2 pieces,). In this case, the weak ballast particles possibly break into smaller pieces. Corner breakage occurs mainly at the condition of ballast particles under low confining pressures, while splitting fracture occurs mainly at high confining pressures [97].

Alternatively, in [18], three types of ballast particle degradation were classified as shown in Fig. 14. This classification can describe sharp corner breakage more easily, because sharp corner breakage can be treated as breakage or abrasion. This classification with three types uses categories according to the ballast shape properties (Fig. 1), which is promising for use in future studies.

The ballast particle also has different types of degradation as forces applied to the particle are different as shown in Fig. 15. From the figure, it can be seen that abrasion/polishing is normally caused by ballast-ballast relative movements, such as rotation, rubbing, etc. In addition, particle breakage is also influenced by the coordination number, which was proved in the study [98].

Ballast particle breakage is one of the main causes (particle degradation and re-arrangement) to permanent differential settlement of the track [99]. Because ballast breakage happens at the places with impact loading or with hanging sleeper, where the sleeper-ballast stress is concentrated at some ballast particles. For that, the ballast particles under the sleeper suffer from unbearable forces, causing not only rapid degradation but also quick re-arrangements. Note that losing the angularities as well as surface roughness are also key reasons for quick re-arrangements. The ballast layer makes the largest contribution to track settlement under the condition of short-term loading-deformation (deformation contribution from subgrade can be neglected), specifically, 50–70% of the total vertical deformation comes from the ballast layer [100]. This was also proved in [101], which showed the cumulative permanent strains of ballasted track on a stiff subgrade, as shown in. Ballast abrasion/wear also happens frequently, especially for high speed railways due to the higher frequency of vibration. In addition, it was stated that ballast abrasion reduces the ballast layer shear strength [21].

Particle abrasion is the phenomenon whereby very small particles are chipped from the surface of larger particles, and is mostly independent of the stress level. It is more related to the ballast layer vibration frequency [102]. It occurs as a result of sliding or rolling between particles due to shear deformation, even at lower stress levels. Although particle compressive strength is not typically mentioned in ballast standards, it is reflected in the testing of ballast breakage and durability.

In [75], LAA tests were performed on limestone ballast particles, and 2D images of these particles were analysed to assess particle degradation. Results showed that large ballast particles were more prone to breakage in the early stages of the LAA test due to the presence of sharp corners and edges. In contrast, the small ballast particles tended to be more spherical in shape and therefore produced less fines from abrasion. At a later stage, as the ballast particles become smoother and more rounded, they accordingly become more resistant to breakage and abrasion. This is consistent with the findings in [4,103,104]. In addition, it was also found that ballast particles with sharp angularities are more likely to suffer more severe deterioration [92].

In [105], direct shear tests were performed on ballast at different levels of degradation. Ballast particle degradation was simulated using LAA tests with different evolutions. The results showed that as particle roundness increases, the peak shear strength of the ballast matrices can slightly improve, however the residual shear strength is substantially reduced. This is because a high value of roundness leads to a small mean coordination number. Additionally, it decreases particle sliding contacts, as well as reduces the mean particle contact moment.

Ballast particle fracture consists of particle breakage and sharp corner fracture, with particle fracture beginning with tensile damage. According to studies [106–108], the tensile breaking strength (σ_f) of ballast particles can be calculated by Eq. (2). In the equation, F_f is the

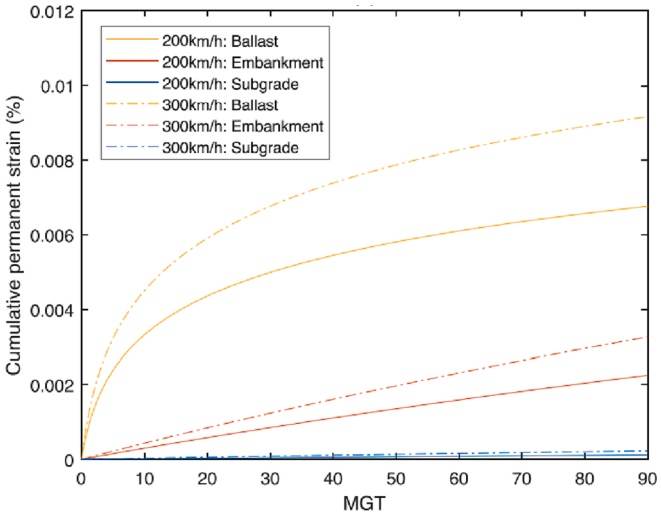

Fig. 16. *Cumulative permanent strain of ballasted track on a stiff subgrade (figure reproduced from [101]).*

applied stress and d is the diameter of ballast particle.

$$\sigma_f = \frac{F_f}{d^2} \tag{2}$$

Particle fracture generally occurs under high stress, thus causing particles to break into similar sized pieces. The pieces have similarity and their size and shape is distributed with some regularity [109].

In [59], direct shear tests were performed on a mix of aged and new ballast after cleaning (Fig. 16). After a long period of operation, new ballast particles are broken, worn and rearranged under cyclic train loading, resulting in rounded particle corners and smooth surfaces, which in turn reduce bearing capacity, resistance and drainage properties. This also causes defects such as ballast layer fouling. To solve these problems, ballast beds need to be regularly screened and renewed. The ballast renewal is performed by mixing new ballast particles into the screened ballast layer. Results show that the shear strength of the new ballast is 58% higher than the shear strength of the deteriorated ballast (ballast degradation is simulated by LAA tests). This shows that ballast particle degradation will significantly reduce the bearing capacity of ballast layer, and ballast renewal is an effective means of improving the bearing capacity of the bed. Because the shear strength of ballast assemblies are mainly provided by the inter-particle friction and interlock forces.

In [110], effects of ballast particle degradation on ballast layer performance were studied. A single-sleeper track model using DEM was

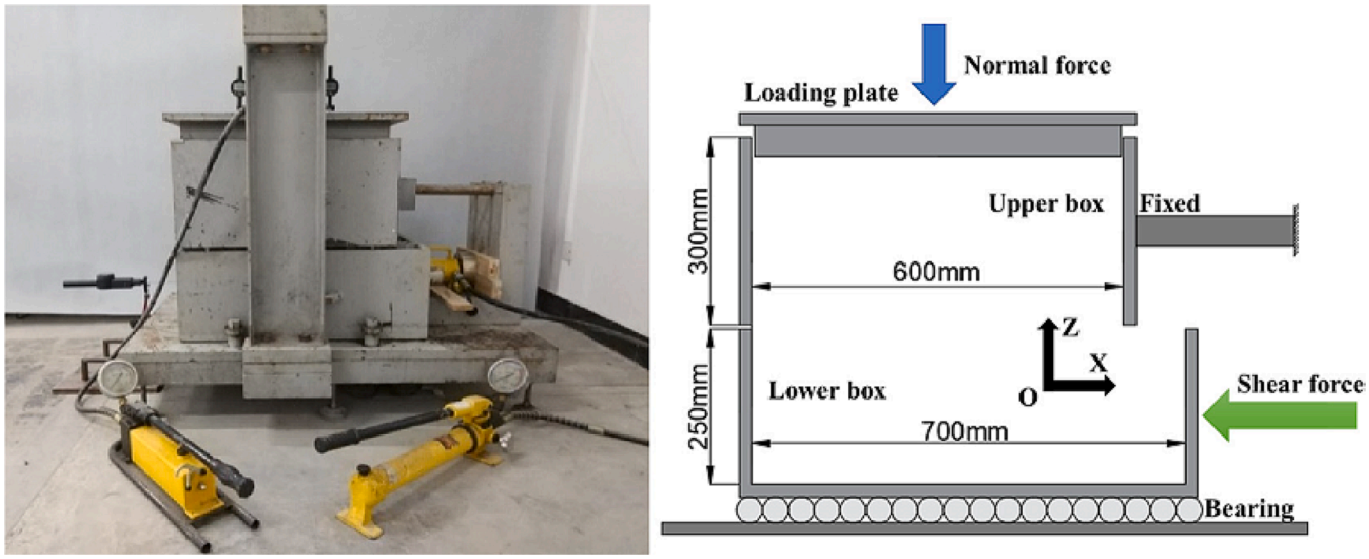

Fig. 17. *Direct shear test box with dimensional sizes: 550*600*700 mm (figure reproduced from [59]).*

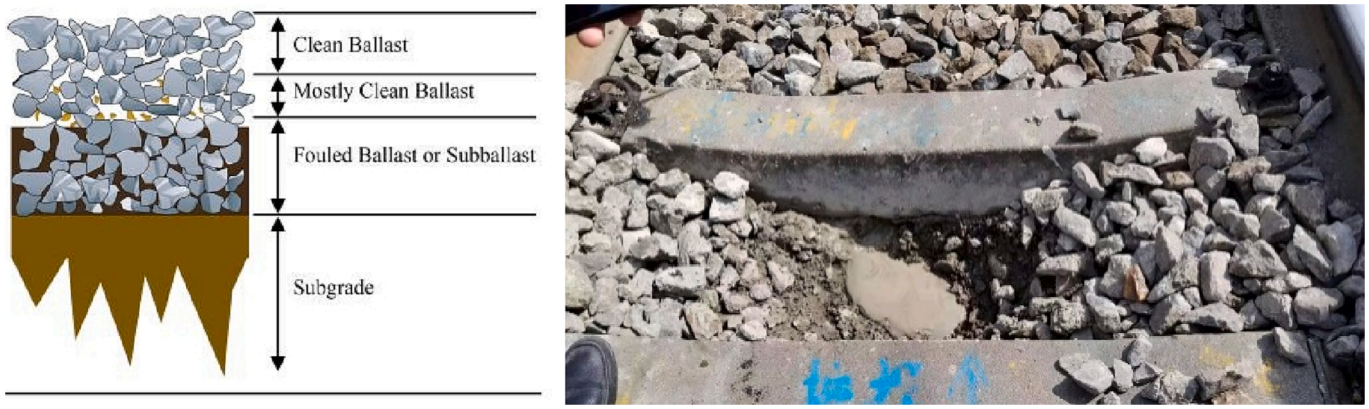

Fig. 18. Ballast layer fouling.

Table 3
Summary of earlier studies on ballast layer fouling.

Factor	Reference	Main conclusion/findings
Fouling percentage	[119,120]	• It was concluded that fouling has a significant effect on the ballast layer performance. The ballast layer cannot contain over 10% or more fines (contamination). mechanical behaviour of ballast with different PSDs and sand contents were studied. Sand fouling increases ballast layer stiffness and reduces ballast particle breakage, additionally settlement and damping ratio of ballast layer are increased.
Water content (moisture)	[114,121–123]	• The increase in water content with increasing ballast layer fouling leads to a sharp increase in ballast layer settlement. Ballast settlement and plastic deformation mostly occur in poor drainage ballast layers due to high fouling levels. The plastic strain of fouled ballast is increased due to lubricated contacts between large ballast particle. Increasing moisture (>3%) leads to large accumulation of plastic strain of ballast. Wet coal fouling substantially exacerbates the shear strength reduction. Approximately 15% coal dust fouling by weight can be the limits as ballast layer fouling. Because In wet coal dust with 35% water content, the friction angle of ballast-coal mixture is as low as that of only coal. Settlement in saturated water-bearing ballast was approximately 40% higher than that in dry ballast.
Fouling material	[100,124,125]	• Ballast layer fouling leads to the rapid ballast layer function failure, which is closely related to the size and quality of the fouling materials. The fouling materials are different due to transportation types. For example, in North America, ballast particle degradation made the greatest contribution to ballast layer fouling. However, in British railways the largest sources of ballast fouling are external wagon spillage and airborne dirt. In Qatar and the GCC countries, it is crucial to consider the presence of sand particles in the ballast layer (from dust storms) and the different maintenance methods used for sand extraction. The peak shear stress of fouled ballast decreases. The fouling can reduce maximum contact force by increasing contact area between two ballast particles, thus reducing breakage of fouled ballast. Coal fouling reduces the shear strength of ballast. Small coordination numbers, low average contact forces and less particle rotations are the reason of shear strength reduction. Uniformly-distributed size (around 26.5 mm) of coal fouling presents large shear stresses than other sizes of coal fouling.

built to study new and deteriorated ballast performance under cyclic loading. Results showed that sleepers on degraded ballast have larger vibrations than on new ballast. Deteriorated ballast shows a frequent stress concentrations in ballast layer, while the new ballast layer has a more uniform force distribution in the ballast under cyclic loading. In addition, greater ballast particle rearrangement was found in the ballast layer containing deteriorated ballast particles.

Table 4
Studies on permeability, evapotranspiration and freeze of ballast layer.

Factor	Reference	Main conclusion/findings
Permeability	[37,126,127]	• The equation correlating hydraulic conductivity (k) with ballast contamination rates (b_{cr}) was proposed as shown in Equation 3. *Equation 3* $k = 0.0324 \times e^{-0.5041 \times b_{cr}}$ Permeability of ballast layer was unacceptable when ballast degradation together with soil contamination happened. A new Permeability Index (PI) was proposed to indicate ballast permeability (factor: ballast layer degradation level). Water flow characteristics in ballast layer have a nonlinear power-curve trend (especially for clean ballast), the discharge velocity of which is related to the hydraulic gradient.
Evapotranspiration	[128]	The potential evapotranspiration of ballast layer is influenced by the temperature and water content. In addition, it can significantly interact with railway ballast properties. It is mostly related to the ballast particle property – weathering resistance, which was estimated by the sulfation test. In addition, frozen ballast layer provide different performance due to the ballast particles are bonded by ice (Fig. 19).
Freeze	[116,128,129]	• The resistances of ballast layer to sleeper in a low temperature environment were different from those in a normal temperature. In dry conditions, with the temperature dropped from −20 °C to −30 °C, the lateral and longitudinal resistance decreased by 28% and 16% respectively. The ballast layer with unfrozen water, the lateral and longitudinal resistances decrease by approximately 22% and 17%, respectively. While the water in ballast layer is frozen, the ice bonds each two contacted ballast particles, which increases the lateral and longitudinal resistances by approximately 128% and 108%, respectively The low temperature has great affects ballast layer vibration responses, because the vibration energy is difficult to dissipate in the frozen ballast layer. In addition, the frozen ballast layer is easily damaged because of the high ballast layer vertical stiffness and low elasticity.

Ballast layer fouling

The voids in the ballast layer provide drainage. However, after long-term service, the accumulation of fouling/contamination in the voids can be one of the key causes of track deterioration, poor alignment and poor drainage [32,111]. Over time, large voids can be filled in with contaminations (e.g. soil, sands fines from ballast abrasion and coal), reducing permeability and increasing moisture in the ballast layer, as shown in Fig. 17. A fouled ballasted layer cannot provide free drainage for the track [112,113]. Most importantly, fouled ballast layers have reduced mechanical performance, for example in terms of vertical support and lateral stability. Further, settlement increases with fouling level [114].

During the deterioration processes, contaminates accumulate from bottom to surface and the ballast layer starts to harden [115]. In fouled ballast layers, the interlock and friction between ballast particles, the interaction between sleeper and ballast, particle pore structure changes, rate of particle fragmentation, environmental corrosion, changes in

Table 5
Factors and mechanical performances for different ballast layer bulk densities.

Factors/Mechanical performance	Reference	Conclusion/findings
PSD	[76]	Increasing ballast layer bulk density reduces the amount of particle breakage and wear.
Initial bulk density	[7,135,136]	High initial porosity leads to high ballast particle degradation when applied train cyclic loading.
Track stability	[133,137]	All the studies on track stability have the same conclusion on that increasing ballast layer bulk density (i.e. reducing porosity) enhances its strength and stability.
Deformation	[100]	Low bulk density ballast layer leads to high plastic deformation of ballast layer.
elasticity modulus	[91,138,139]	The effect of porosity on the elasticity modulus of ballast was minimal. The effect of bulk density on the elastic properties of ballast still needs more studies to reveal it.

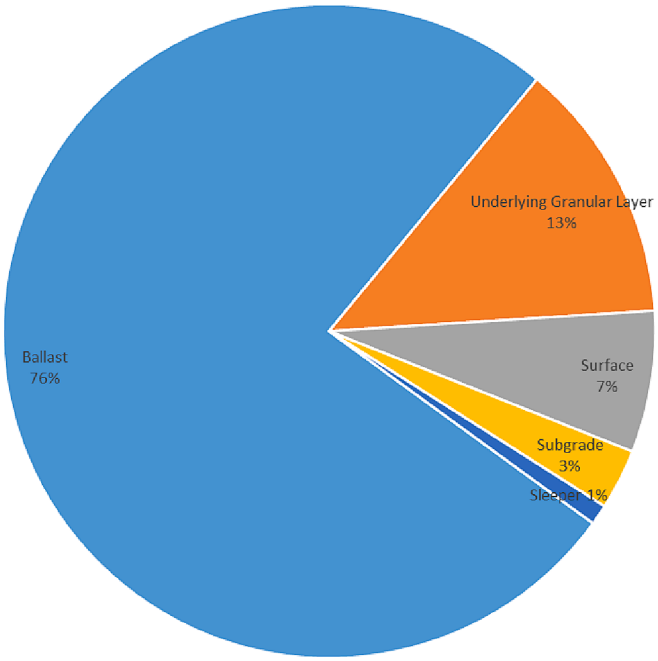

Fig. 19. Sources of ballast layer fouling.

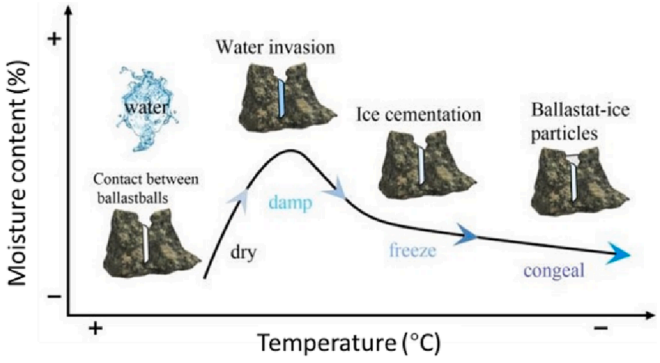

Fig. 20. *Interaction between ballast and water/ice* [128].

water content and accumulation of external contaminations, etc., are different from clean ballast layers. A problem caused by fouling is that the ballast layer density increases, resulting in a reduction of elasticity

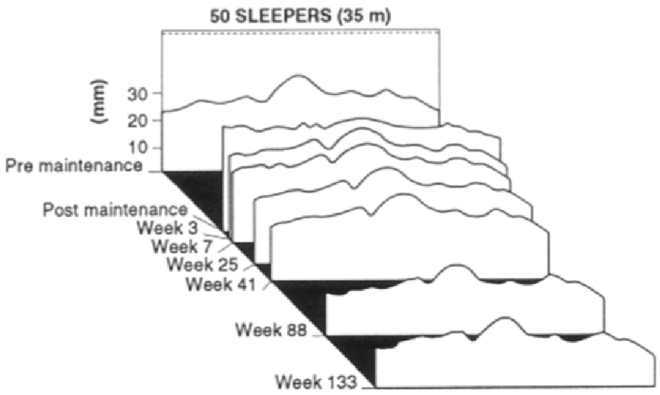

Fig. 21. *Ballast memory caused similar track geometry degradation (figure reproduced from* [100]*).*

Table 6
Mechanical properties of ballast layer under different frequencies of loading.

Loading frequency (f)	Mechanical properties of ballast layer
f < 25 Hz	Solid characteristics, high resistance from ballast layer to sleeper
25 Hz < f < 50 Hz	Sticky characteristics, relatively low resistance from ballast layer to sleeper
f > 50 Hz	Fluid characteristics, complete fluidisation of ballast particles, loss of load-bearing capacity

Table 7
Effect of ballast layer bulk density, friction coefficient on ballast vibration [156,157].

Ballast layer properties		Ballast vibration speed (mm/s)	Ballast acceleration (mm/s2)
Bulk density (kg/m3)	1700	17.84	16.74
	1800	15.80	14.82
	1900	12.83	14.40
	2000	12.19	9.65
Friction coefficient	0.4	19.46	17.43
	0.5	18.48	15.65
	0.6	15.37	14.96
	0.7	12.83	14.40
	0.8	11.42	9.76

Table 8
Ballast acceleration and vibration acceleration of ballast at different ballast layer depths [156,157].

Ballast layer depth (m)	Ballast vibration speed (mm/s)	Ballast acceleration (mm/s2)
0.05	12.83	14.10
0.15	11.71	9.41
0.25	6.94	3.32
0.35	3.03	2.54

and load-bearing capacity. It is also important to note that freeze–thaw can occur on cold railway lines, leading to sharp changes in track stiffness [116]. This uneven track stiffness and settlement causes damage to the track components as well as sub-structure.

Fouled ballast layers make it difficult to maintain track geometry. Poor drainage causes rainwater to accumulate at the interface of ballast and subgrade which can cause mud-pumping and track geometry deterioration. Heavily fouled ballast layers that are maintained by tamping and stabilisation can result in further damage to the ballast layer thus

Table 9
Ballast layer vibration generation and measurement methods.

Methods	Reference	Conclusion/findings
Shaking table	[158–160]	A scaled ballasted track model was used to simulate the ballast-sleeper interaction under seismic loading, as shown in Fig. 21. Restricting the track at longitudinal direction can improve the natural frequency of bridges, which can reduce the bridge vibration. The ballast layer collapses (fluidisation) due to the seismic loading makes track stability complex. Lateral resistance decreases sharply during the shaking process and the ballast layer profile did not change significantly after the shaking.
SmartRock	[161–163]	SmartRock is an accelerometer with an irregular-shaped cover, which can move freely as real ballast particle. Horizontal movement and rotation are main ballast particle movements under cyclic loading. The fouled ballast layer has poor performance when water is involved. The ballast particle movements can reflect ballast layer fouling and shoulder instability. Increasing loading frequency reduces the interlocks between particles. Increasing loading magnitude increases the particle contact forces and accelerations beneath sleeper end.
DEM modelling	[164–166]	• Ballast particles that are 200 mm below sleepers are disturbed under train loading. The acceleration amplitudes rise sharply on the condition of vehicle speed over 200 km/h. The dominant frequencies of are less than 100 Hz. Modifying ballast layer stiffness with crumb rubber has few effects on train dynamic responses, while crumb rubber can consume energy transferred to ballast layer, reducing ballast layer degradation. Ballast natural frequency is over 1000 Hz, while ballast layer natural frequency is lower. The vertical acceleration transmission (frequency < 257.94 Hz) in ballast layer is low. Vibration suppression ability of the ballasted bed is better in the lower frequency range.
Accelerometer	[44,96,167]	• The ballast layer acceleration was used to calibrate and validate the train-track model built with multibody dynamics. Ballast layer acceleration is affected also by the track structure, especially when changing the track stiffness. Installing under sleeper pads of improper stiffness can even increase the ballast layer acceleration. Sleeper-ballast interface accelerations at 100–1000 Hz (caused by impact loading), which can be substantially consumed by the ballast layer due to its high rigidity. However, the ballast layer can only slightly consume the vibration lower than 100 Hz.

reducing the maintenance cycle [2].

It is generally accepted that the ballast layer is heavily fouled when the fine mass percentage of 14 mm exceeds 30%, which is normally used as an indicator for ballast layer maintenance (sieving and renewal) [117]. New ballast layers after construction have the fouling percentage between 3% and 5%.

Different sources of fouling material in railway ballast are shown in Fig. 18. The main sources of fouling materials are: ballast particle degradation (76%), infiltration from sub-ballast (13%), ballast surface infiltration (7%), subgrade infiltration (3%) and sleeper degradation (1%). Ballast particle degradation is caused by: transportation, thermal stress, chemical weathering, tamping, stabilisation and traffic loading. The main contamination is fine or small particles generated by ballast abrasion or breakage. Infiltration of subgrade and sub-ballast layers into the ballast are caused when the ballast layer is pressed into the subgrade. For example, below the rail at the ballast-subgrade interface, ballast pockets can occur [100].

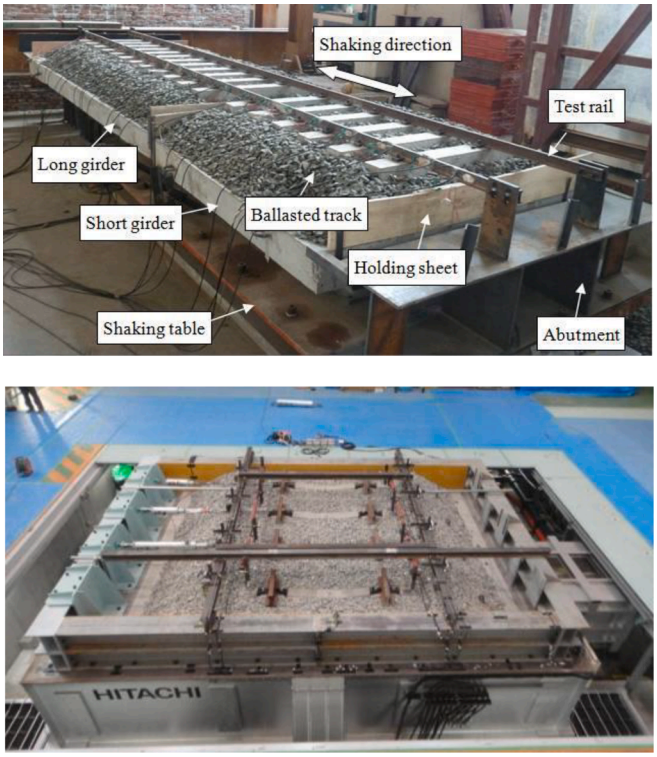

Fig. 22. Scaled ballasted track model on shaking table *(reproduced from* [159,160]*)*.

The extent of negative effects of fouling on the mechanical behaviour of the ballast layer depends on several factors, such as fouling material, water content and fouling percentage (fouling level) [118]. In Table 3, earlier studies are summarised and classified.

Ballast permeability

The water content (ballast layer moisture) influences the mechanical performance of ballast layer under dynamic loadings. Water moves in the ballast layer, as well is absorbed by ballast. The water entering the micro-cracks in the ballast particles at the ballast-ballast contacts increases the local stress on the ballast and leads to an increase in particle degradation. Therefore, ballast drainage (permeability) is important factor influencing potential evapotranspiration.

In earlier studies (e.g. Table 4), the permeability of ballast was investigated. In addition, in low temperature, the evapotranspiration and freeze of ballast layer were studied. Limited studies have been performed on correlating drainage with ballast layer performance.

Bulk density/porosity and dynamics

Ballast layer bulk density/porosity

The ratio of pore volume to solid volume, i.e. porosity, has a significant effect on the mechanical properties of granular materials [130–132]. On this basis, in [7,133] the theory was extended to railway ballast, arguing that the strength and stability of the ballast layer increases when the ballast layer has a high bulk density (or relative density), i.e. a low porosity. At this point the shear strength of the ballast assemblies is maximised and the deformation (especially settlement) is minimised. The effect of bulk density on elastic modulus have still not reached the conclusion.

The effect of density is more significant for partially crushed stone than fully crushed rock. The rebound modulus of partially crushed rock

Table 10
Test procedure and main test purpose.

Single particle crush test	One ballast particle is placed between two steel panels, and slowly pressing the ballast particle until it is crushed.	The test purpose of single particle crush test is to obtain the types of particle crush, the material strength (curve of force–displacement and the size-related failure pressure) [168].
Angle of repose test	A cylinder container is filled with ballast particles, afterwards, pouring the ballast particles down to measure the repose angle. The angle of the small ballast particle hill is the angle of repose, which is used to reflect the internal friction angle.	The test purpose is to obtain the angle of repose, which is an indicator of internal friction angle. The test results are dependent on the material (e.g., density), particle shape (roughness, angularity and form) and particle size distribution (PSD, or gradation) [63].
Compression test	Compression test has two types. One is the confined compression test. Confined compression test is fully filling ballast particles in a cylinder or box, and using hydraulic jack to press a plate that is placed on the top of the ballast assemblies in the cylinder or box. The other is unconfined compression test. It is used for treated ballast assemblies by e.g., polyurethane and asphalt [171,172].	The cylinder or box is a container that has fixed boundary. The test purpose is to obtain the curve of force–displacement. It can be used for testing compression strength of ballast assemblies. The test results are dependent on the material, particle shape, compaction (bulk density or porosity) and gradation.
Direct shear test	Two shear boxes are filled with ballast particles, and using hydraulic jack to push one shear box. The top plate that is placed on the ballast sample is loaded by a consistent vertical stress. The top plate is free to move at vertical direction, which can measure the shear dilation of ballast assemblies.	The test purpose is to obtain the shear strength of ballast assemblies under various vertical stresses, presented by curve of stress–strain. The volumetric change behaviour is tested by the measuring the dilation of ballast assemblies. Particularly, the direct shear tests were applied to understand the factors influencing the shear strength of ballast assemblies, e.g., particle shape (elongation and flakiness) [74], ballast material [59] and fouling (percentage, type) [114,124].
Los Angeles Abrasion test	12 steel balls and ballast particles (5 or 10 kg) are put into the test machine cylinder, and then rotate the cylinder at some turns (500, 1.000). The rotation speed is at 31–33 r/min.	Los Angeles Abrasion test is used for analysing durability and strength of ballast particles. The mass loss (by weight percentage) that is particles under 1.6 mm is used to present the ballast material properties (durability and strength). The Los Angeles Abrasion tests have been applied to understand the factors influencing the strength of ballast assemblies, e.g., particle shape, particle size and ballast material [4,9,173].

increases with increasing bulk density, while increasing bulk density of fully crushed rock has little effect on the modulus of resilience. This is because partially crushed rock is less angular than fully crushed rock [134].

Related studies on ballast layer bulk density/porosity are given in Table 5. The factors (PSD, ballast particle degradation and ballast material) or mechanical performances (track stability, deformation) are listed.

Track stability can be improved by increasing the bulk density of the ballast layer through further compaction or by using ballast with a wide PSD. However, higher compaction levels also increase the risk of ballast breakage (especially for heavy haul), a wide PSD can lead to reduced ballast layer drainage.

Table 11
Comparison of largest ballast particle size to sample size ratio.

Test name	Largest particle size (mm)	Sample size (mm)	Ratio
Angle of repose test [174]	62.5	400	1/6.4
Unconfined compression test [175]	62.5	200	1/3.2
Direct shear test [124]	25	200	1/8
Direct shear test [59]	63	600	1/9.5

An advantage of high density railway ballast is that it can reduce ballast flight on high-speed railway lines. However, limited studies have been performed on the field bulk density or porosity because they are hard to measure. 3D ground penetrating radar (GPR) maybe a promising to achieve this. More explanations about GPR application to railway ballast layer inspection can be found in [140–142].

Ballast layer dynamics

High speed trains can generate high frequency impact loads, which act on the ballast. The impact loads are transferred to the sleepers via the rails and then dispersed by the sleepers to the ballast layer, causing continuous vibration within the ballast layer. This vibration is a cause of ballast particle degradation and ballast layer fouling. The high frequency vibration of the ballast layer and the joint action of the wind load of the train may also cause the ballast flight, potentially endangering the train operational safety [143].

Ballast memory is phenomenon where the vertical track geometry returns to its original form after maintenance, as shown in Fig. 20. This phenomenon is related with ballast layer dynamics however can be minimised by performing dynamic track stabilisation after tamping [144].

Ballast layers on a bridge (or other high-stiffness sub-structure) are subject to high frequency vibration under train loading, which causes the ballast layer to flow [145]. Therefore, it is necessary to study the ballast layer dynamic response, especially under high speed train loading.

Ballast layer dynamic response on bridges

Ballast layer flow refers to the liquid-like flow of ballast particles near a resonant frequency [96]. This phenomenon more frequently happens in the ballast on bridges when vehicle speeds reach 200 km/h and above [146]. The flow deformation of ballast leads to a deterioration in track instability and geometry. Most importantly, it reduces the lateral resistance between the ballast and sleepers, potentially affecting the safety of vehicle operation. In addition, rapid ballast particle degradation (dominantly abrasion) on the bridge also produces large amounts of dusts.

These problems result from the dynamic response of the ballast layer. Solutions regarding structural and mechanical optimisation were proposed, such as ballast mats and retaining walls for ballast [147,148]. In [146,149,150], systematic studies were performed on the dynamics of ballast layers on bridges. Results show that as the loading frequency increases, the mechanical properties of the ballast gradually transform from quasi-solid to quasi-fluid (Table 6), which is consistent with the results obtained through field experiments.

Fluid characteristics (fluidisation) is from vertical accelerations exceeding 0.7–0.8 g, which is caused by trains passing over the bridge at a speed capable of exciting the natural frequencies of the system [151]. In addition, when regular wheel pairs are running at a certain speed, they may resonate with the bridge, which is also the main source of

a. Single particle crush test (reproduced from [168])

b. Angle of repose test (reproduced from [169])

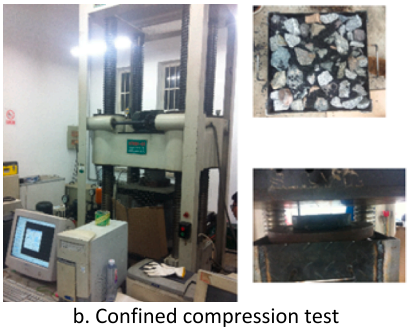

b. Confined compression test

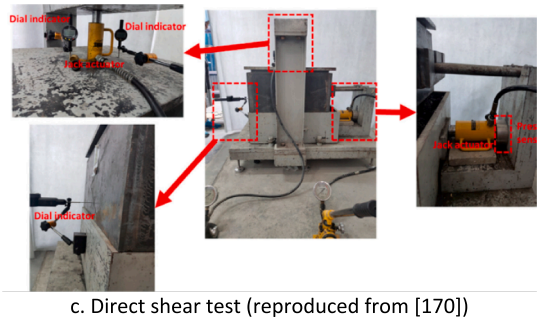

c. Direct shear test (reproduced from [170])

e. Los Angeles Abrasion test (reproduced from [16])

Fig. 23. Apparatus for classic mechanical tests.

fluidisation. It is therefore important to check that the vertical acceleration applied to the ballast layer does not exceed 0.35 g (safety factor 2) and that the frequency range is below 20 Hz [152]. Note that the normal open track ballast acceleration is lower than that on the bridge. Because the ballast on bridge cannot give its energy to the subgrade, but to the bridge. The bridge has much higher stiffness than subgrade, for which the residual energy of ballast leads to more vibrations. Another reason is that the single ballast acceleration is different from ballast layer acceleration. Ballast layer acceleration is decided by the ballast layer stiffness. Single ballast particle acceleration is decided by the ballast material as well as the coordination number of the ballast particle. Coordination number is the contacts to its neighbouring ballast particles.

After checking the dynamic response parameters of the train-track-bridge structure (stiffness, natural frequency, damping, etc.), the relationship between the structural characteristics and ballast fluidisation can be analysed [151,153,154]. Afterwards, specific measures (e.g. application of wider sleepers, under sleeper pads, ballast cleaning, etc.) for ballasted track can reduce the vibration acceleration of bridges and reduce the probability and amplitude of ballast fluidisation [152,155].

Ballast layer vibration

Ballast layer vibration is linked to ballast layer deterioration, because the main means of dissipating train loading in the ballast layer is through friction. Deteriorated ballast particles have lower friction. High compaction leads to more contacts between ballast particles, thus higher ballast-ballast friction. Therefore, it is important to study the porosity (corresponding bulk density, relative density) and friction coefficient on vibration in ballast layer.

Ballast layer vibration has been studied using DEM modelling, for example, in [156]. At a depth of 0.05 m below the sleeper, the vibration speed and acceleration of ballast at different ballast layer bulk densities and ballast friction coefficients were compared, as shown in Table 7. Results showed that the ballast vibration speed and acceleration decreased with increasing bed density and friction coefficient.

Ballast layer vibration is transmitted and dissipated from the top to the bottom of the ballast layer. Particle acceleration and vibration acceleration of ballast at different depths under cyclic loading of the rail sleeper were studied in [156,157], as shown in Table 8. Results show that as the depth of the bed increases, the velocity of the ballast particles decreases from 12.83 mm/s at the surface to 3.03 mm/s at the bottom - a reduction of 76.4%. The acceleration of the ballast particles decreases from 14.40 mm/s^2 at the surface to 2.54 mm/s^2 at the bottom - a reduction of 82.4%.

As shown in Table 9, studies on ballast layer vibration methods and

(a) Triaxial test (reproduced from [177])

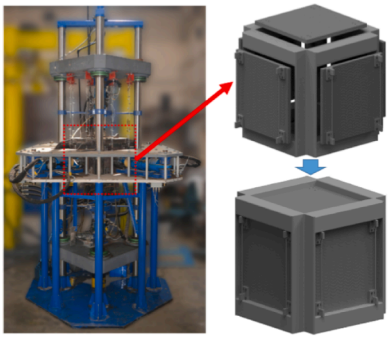

(b) True triaxial test (modified after [178])

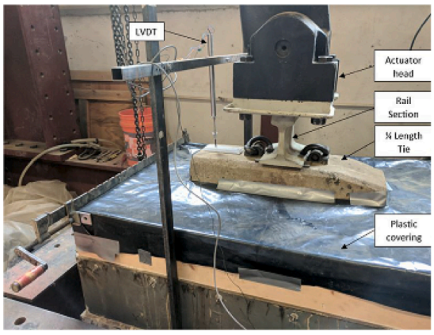

(c) Ballast box test (reproduced from [87])

(d) Large-scale process simulation test (reproduced from [179])

(e) Full-scale ballasted track model (reproduced from [180])

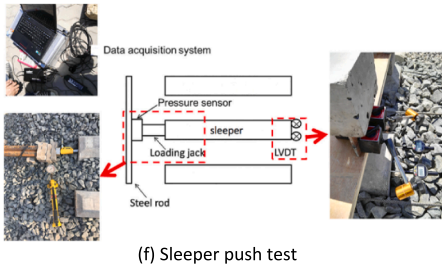

(f) Sleeper push test

(g) Pull-out test (reproduced from [181])

Fig. 24. Test setups of field tests and full-scale track tests.

Table A1
Classical mechanical tests.

Test name	References	Sample dimension and particle size	Loading	Test result; research contents
Single particle crush test	Dahal and Mishra, 2020 [19]	None / 40, 45, 58 mm	1.9 mm/s	Three kinds of ballast materials were compared. The validated particles were used for the ballast box test model.
Single particle crush test	Wang et al., 2017 [15]	None / 40, 45, 50 mm	0.5 mm/min	Ballast particle shape was considered, including cubic, elongated and flaky particles. A new sphere-bonding method to make crushable particles was applied.
Angle of repose test	Xiao et al., 2019 [169]	Sample: 250 mm diameter; 900 mm height. Particle: 22–62.5 mm	–	Repose angle: (39.78 ± 1.27)°. Validated parameters are used for single sleeper push test model.
Angle of repose test	Fu et al., 2020 [216]	Sample: a cylindrical hopper (500 mm diameter) connected with an open cone at the bottom (200 mm diameter). Particle: mean size D_{50} of 40 mm.	–	Repose angle: 37.1–39.3°. Influence of particle shape (roughness, angularity and form) on the repose angle.
Angle of repose test	Zhao et al., 2020a [174]	Sample: 400 mm diameter; height not-mentioned. Particle: 16–62.5 mm.	–	Repose angle: 32.5°. Validated parameters are used for direct shear test model.
Unconfined compression test	Liu et al., 2020 [175]	Sample: box – 200 × 200 × 200 mm. Particle: 16–62.5 mm.	1.2 kN/s	Ballast-ice combinations were pressed. The validated DEM model was used to analyses bond breakage.
Confined compression test	Suhr et al., 2018 [217]	Sample: box – 300 × 300 × 200 mm. Particle: 20–40 mm	Only the upper side of sample is applied step-loading, 10, 15, 20, 25 and 30 kN (around 13 min)	Two ballast materials(Calcite and Limestone). Particles of simple shapes with the Conical Damage Model contact model was proved better than Hertz-Mindlin contact model.
Direct shear test	Indraratna et al., 2012 [124]	Sample: box – 300 × 300 × 200 mm. Particle: ballast, 2–25 mm; fouling, 0.1–10 mm	Shearing speed: 0.04 mm/s. Vertical load: 27, 51, 75 kPa	Shear behaviour of fresh and fouled ballast was studied. Validated DEM models were used to present distribution of contact force chains and particle displacement vectors.
Direct shear test	Jia et al., 2019 [59]	Sample: lower box – 600 × 700 × 250 mm; upper box – 600 × 600 × 300 mm. Particle: 22.4–63 mm	Shearing speed: 0.3 mm/min. Vertical load: 50, 100, 200 kPa	Performance of mixture of new and old ballast was studied. Validated DEM models were used to present shear strength, contact forces, coordination numbers and displacements of ballast particles.
Direct shear test	Gong et al., 2019 [218]	Sample: box – 500 × 500 × 350 mm; Particle: 5–63.5 mm	Shearing speed: 2 mm/min. Vertical load: 50, 100, 150 kPa	Shear strength of mixture of tire derived and ballast was studied. Validated DEM models were used to study aggregates coordination number (CN) and contact force distribution.
Direct shear test	Ngo et al., 2014, 2016 [176,219]	Sample: box – 300 × 300 × 200 mm. Particle: ballast, 2–25 mm; fouling, 0.1–10 mm	Shearing speed: 0.04 mm/s. Vertical load: 27, 51, 75 kPa	Shear behaviour of fresh and fouled ballast with geogrid was studied. Validated DEM models were used to present contact force chains and contact force distribution and contours of strain developed in the geogrids.
Direct shear test	Wang et al., 2015 [60]	Sample: box – 300 × 360 × 240 mm. Particle: 22–60 mm	Shearing speed: Not-mentioned. Vertical load: 100, 200, 300 kPa	Validated DEM models were used to present contact force chains, coordination number and particle displacements. Two particle size distributions of ballast samples were compared.
Direct shear test	Danesh et al., 2020 [71]	Sample: box – 310 × 310 × 210 mm. Particle: 30 mm	Shearing speed: Not-mentioned. Vertical load: 50, 300 kPa	Validated DEM models were used to present contact force chains and particle rotations. The particle shape (angularity and sphericity) influence on shear strength was studied.
Direct shear test	Huang and Tutumluer, 2011 [114]	Sample: lower box – 365 × 305 × 152 mm; upper box – 305 × 305 × 51 mm. Particle: 12.5–76.2 mm	Shearing speed: 0.2 mm/s Vertical load: 172, 241, 310 kPa	Shear behaviour of fresh and fouled ballast was studied. Validated direct shear test model was used to present contact forces. Using the validated parameters, a half-track model was built to study fouled ballast bed settlement.
Direct shear test	Bian et al., 2019 [80]	Sample: lower box – 365 × 305 × 152 mm; upper box – 305 × 305 × 51 mm. Particle: 12.5–76.2 mm	Shearing speed: 12.2 mm/min Vertical load: 158, 248, 317 kPa	Validated DEM models were used to present contact force chains, coordination number, particle displacements and particle rotations. Effects of particle size effects in relation to shear box test equipment dimensions, porosity and particle shapes on shear strength was studied.
Direct shear test	Guo et al., 2020 [170]	Sample: lower box – 600 × 700 × 250 mm; upper box – 600 × 600 × 300 mm. Particle: 22.4–63 mm	Shearing speed: 0.3 mm/min. Vertical load: 50, 100, 200 kPa	Shear behaviour of Neoballast was studied. Validated DEM models were used to present contact force chains, and particle displacements. Using the validated parameters, a three-sleeper track model was built to study the settlement, particle displacements and acceleration of ballast bed with Neoballast.
Direct shear test	Suhr et al., 2018 [217]	Sample: box – 300 × 300 × 200 mm. Particle: 20–40 mm	Shearing speed: 1 mm/min Vertical load: 10, 20, 30 kN	Two ballast materials(Calcite and Limestone). Particles of simple shapes with the Conical Damage Model contact model was proved better than Hertz-Mindlin contact model.
Triaxial test	Harkness et al., 2016 [220]	Sample: 150 mm diameter; 300 mm height. Particle: 7.47–20.83 mm	Axial load speed: Not-mentioned Confining pressures: 15, 30, 200 kPa	The test was used to validate a new contact model, which models damages at the contacts between ballast particles. The contacts were simulated as spherically-capped cone. The yield stress crushes the cap into a lower cap with a larger radius.
Triaxial test	Liu et al., 2019 [221]	Sample: 305 mm diameter; 610 mm height. Particle: 9.5–50 mm	Axial load speed: 0.051 mm/s Confining pressures: 55, 110, 165 kPa	Using the SmartRock to calibrate DEM model.

(*continued on next page*)

Table A1 (*continued*)

Test name	References	Sample dimension and particle size	Loading	Test result; research contents
Triaxial test	Ngo and Indraratna, 2017, 2020 [184,222]	Sample: 300 mm diameter; 600 mm height. Particle: 10–60 mm	Axial load speed: 0.55 mm/min Confining pressures: 10, 30, 60 kPa	Shear behaviour of fresh and fouled ballast was studied. Validated DEM models were used to study particle breakage, contact coordination number, deviatoric fabric, contact forces, and the associated broken bonds.
Triaxial Test	Qian et al., 2015 [186,187]	Sample: 305 mm diameter; 610 mm height. Particle: 12.5–75 mm	Axial load speed: 30.5 mm/s Confining pressures: 69, 138, 207 kPa	Shear behaviour of ballast particles enforced by geogrid was studied. Validated DEM models were used to study various geogrid properties, such as the aperture shape and size and rib dimensions.
Triaxial Test	Qian et al., 2015 [35]	Sample: 305 mm diameter; 610 mm height. Particle: 12.5–75 mm	Axial load speed: 30.5 mm/s Confining pressures: 69, 138, 207 kPa	Shear behaviour of fresh and fouled ballast enforced by geogrid was studied. Validated DEM models were used to demonstrate ballast reinforcement phenomenon by the geogrid.
Triaxial Test	Qian et al., 2018 [223]	Sample: 305 mm diameter; 610 mm height. Particle: 12.5–75 mm	Axial load speed: 0.1 mm/s Confining pressures: 69 kPa	Validated DEM model was used to study the influence of initial particle arrangement of ballast particles on shear behaviour.
Los Angeles Abrasion test	Xu et al., 2020 [16]	Sample: - Particle: 22.4–63 mm	Dead weight of ballast and steel balls	DEM LAA test model was validated by the LAA ratio. The non-cubic shape ballast particles consumed high kinetic energy, which indicated they reduce the ballast layer stability.

findings are summarised. The methods include creating ballast layer vibration methods (e.g. shaking table) and ballast layer vibration measurement methods, such as using SmartRocks, DEM modelling and accelerometers.

Testing methods

Smaller-scale laboratory tests

Table A. 1 (appendix) shows classic mechanical laboratory tests for assessing ballast performance, with the figures of the apparatus shown in Fig. 22. The sample dimension is the size of ballast sample that is placed in the test rig, while the particle size is usually the particle size distribution. The loading is the forces or stresses applied to the ballast sample.

More details about the classic mechanical tests for railway ballast are given in Table 10, which includes the test procedure and test purpose.

Sample sizes

Sample dimensions are vary between different tests and in-part dictated by the apparatus geometry. Even though similar tests were performed by different researchers, the sample dimensions were different due to variations in the apparatus. It was proposed that when sample size is small relative to the size of ballast particles, the results are less conclusive [7]. Note that earlier studies have confirmed that when the apparatus dimension is at least 6–7 times larger than particle size, the size effect reduces (e.g. Fig. 16). This phenomenon is usually termed the scale effect. Several examples about sample size against largest ballast particle size are compared in Table 11. For the test sample (limited by the test rig size), it is better to use 25–35 mm in the condition that sample size is around 200–300 mm.

As an example, ballast particle sizes are in the range of 20–60 mm [50], which means the biggest ballast particle size is approximately 60 mm. However, in some tests, the apparatuses have been used which are only 300 mm length, which is less than 6 times than particle size. For this, the ballast particles with size at 30–40 mm were applied in the tests, e.g. [176].

From the introduction, it can be seen the sample dimension and ballast particle size range are necessary conditions to obtain reliable results, thus, they are summarised in details in Table A. 1.

Larger-scale track model tests

Test summaries

Table A. 2 (appendix), shows laboratory tests, field tests and full-scale track tests applied for assessing ballast performance. The figures of the test setups are shown in Fig. 23.Fig. 24

The structure of these tests are:

- Triaxial tests: (a) cyclic triaxial test; (b) true triaxial test.
- Ballast box tests: (c) constrained boundaries; (d) movable boundaries.
- Large-scale track tests: (e) vertical loading; (f-g) lateral loading.

Corresponding to Fig. 23:

(a) Large-diameter triaxial test. This test improves upon the triaxial test by applying monotonic or cyclic loading to the cylinder ballast sample. The axial strain, volumetric strain and axial stress are measured. The confining pressure to the ballast sample is provided by compressed air [35,52,182–187].

(b) True triaxial test. The true triaxial test rig was developed in [178], which is a ballast box with 6 movable walls to provide different constant confine pressures in three directions. In addition, cyclic loading can be applied at any direction. This can simulate the complex stresses that act on ballast assemblies in the field. The deformations in three directions (strains) and applied forces are measured.

(c) Ballast box test. Normally an open box that contains ballast particles. An actuator is used to apply cyclic loading to rail or sleeper. During cyclic loading, ballast layer settlement is measured by a dial indicator. In addition, some other instruments can also be installed to measure the concerned ballast layer information (e.g. acceleration, stress under sleeper, etc.) [188–192].

(d) Large-scale process simulation test. Developed by Indraratna [193], the side walls of the ballast box can provide constant stress to ballast sample with adjustable movements. It can also be seen as a combination of a ballast box test and a true triaxial test. One actuator on the top is used to apply cyclic loading, and four actuators are used to control the stress to the ballast.

(e) Full-scale ballasted track model. The model is built with subgrade, a ballast layer and sleepers, and sometimes the rail and fastening system are also installed [194–199]. Actuators are used to apply phased cyclic forces. Normally the sinusoidal cyclic loading with frequency and amplitude simulating the field condition is applied. Some studies simplify the ballasted track model into half-sleeper track model or 1/3 sleeper track model. Some studies applied the scaled track model.

(f) Sleeper push test. This test can be performed by pushing the sleeper in two directions (lateral and longitudinal directions). A hydraulic jack is used to push the sleeper and a dial indicator is used to measure the sleeper displacements [42,200–202].

(g) Pull-out test. This test rig is made using a ballast box with one side containing a gap. It is used mostly for testing the performance of geogrid. Using the actuator, the geogrid is pulled out from the ballast box

Table A2
Field tests and ballast track model tests.

Test name	References	Sample dimension and particle size	Loading	Test result
Large-scale process simulation test	Ngo et al., 2016 [219]	Sample: 800 × 600 × 600 mm Particle: 22.4–63 mm	Cyclic loading: frequency, 15 Hz; amplitude, 420 kPa. Lateral pressure: 10 kPa, 7 kPa.	DEM model was validated by the settlement and wall displacements. Geogrid increased the shear strength and reduced ballast dilation.
Pull-out test	Chen et al., 2014 [181]	Sample: 600 × 400 × 400 mm Particle: 22.4–63 mm	Pumped two times per mm.	DEM model was validated by the pullout forces. A recommendation of particle shape (8-ball tetrahedral clumps) was given.
Cyclic triaxial test	Indraratna et al., 2019 [224]	Sample: 300 mm diameter; 600 mm height. Particle: 2.36–63 mm	Cyclic loading: frequency, 10–40 Hz; amplitude, 230 kPa. Confining pressure: 20 kPa.	DEM model was coupled with finite difference method model. The model was validated by the axial train. Using rubber energy-absorbing mats can reduce the ballast breakage up to about 35%.
Cyclic triaxial test	Indraratna et al., 2009 [225]	Sample: 300 mm diameter; 600 mm height. Particle: 2.36–63 mm	Cyclic loading: frequency, 10–40 Hz; amplitude, 230 kPa. Confining pressure: 374, 428, 482, 536 kPa.	DEM model is validated by observing, which is the response of the ballast during cyclic loading is very similar to that obtained in laboratory experiments. Plastic deformation and ballast particle degradation increased with the loading frequency and cycles.
Ballast box test	Laryea et al., 2014 [226]	Sample: 700 × 450 × 300 mm Particle: 22.4–63 mm	Cyclic loading: frequency, 3 Hz; amplitude, 3 to 40 kN.	DEM model validation was not mentioned. The comparison of steel sleeper and concrete sleeper was performed. The steel sleeper had less settlement over a short period.
Cyclic triaxial tests	Fardin Rosa et al., 2020 [86]	Sample: 150 mm diameter; 300 mm height. Particle: 4.75–31.5 mm (14 PSDs)	Cyclic loading: frequency, 2 Hz; amplitude, 200 kPa. Confining pressure: 40 kPa.	DEM model validation was not mentioned. Considering ballast material is necessary to evaluate ballast layer performance, ballast samples with same PSDs but different materials shows high uncertainties about the ballast performance.
Cyclic triaxial test	Xiao et al., 2017; Xiao et al., 2020 [177,227]	Sample: 300 mm diameter; 600 mm height. Particle: 16–63 mm	Cyclic loading: frequency, 5, 10 Hz; amplitude, 50 kPa. Confining pressure: 30, 60 kPa.	DEM model was validated by matching the axial cumulative strain. A empirical expression involving the maximum principal stress and the ratios of maximum principal stress to minimum principal stress was established.
Full scale track model	Aursudkij et al., 2009 [192]	Sample: 2.1 × 4.1 × 1.9 m; 3 sleepers. Particle: 22.4–50 mm	Cyclic loading: frequency, 3 Hz; 94 kN with a 90° phase lag between each actuator	The stress conditions to ballast layer of the track model are similar to a triaxial test, in which the 30 kPa confining stress was applied with ratio of principal stress to deviator stress between 1.96 and 2.13.
Full scale track model	Feng et al., 2019 [228]	Sample: 15 × 5.5 × 3.7 m; 8 sleepers. Particle: 16–63 mm	Cyclic loading of three train speeds: 108, 252 and 300 km/h with the maximum force at 80 kN	DEM model was validated by comparing the ballast particle vibration velocity and sleeper vibration velocity.
Sleeper push test	Khatibi et al., 2017 [229]	Sample: Field measurement Particle: 12.7–60 mm	Loading is slow from jack, which can be seen as quasi-static loading.	DEM model was validated by comparing the lateral resistance-displacement curve. The ballast layer porosity is the most dominating parameter for ballast layer stability (lateral resistance).
Sleeper push test	Esmaeili et al., 2018 [230]	Sample: 3 sleepers Particle: 12.7–63.5 mm	Loading is from a hammer falling at a desirable triggering angle.	The maximum forces at ballast-sleeper interaction under impact loading are concrete-40 kN, wooden-12.5 kN and steel sleepers-8.5 kN.
Field test (hammer test)	Li et al., 2019 [231]	Sample: Field measurement Particle: not-mentioned	Impact loading from a hammer.	DEM model was validated by comparing the vibrations of sleeper and ballast-subgrade interface. The force chains in ballast layer are influenced by the sleeper shape. Sleeper shape has great influence on the ballast layer contact force chain and the energy propagation in ballast layer.
Full-scale track model	Zhang et al., 2019 [232]	Sample: 8.15 × 6 × 3 m, 13 sleepers. Particle: 22.4–63 mm	Cyclic loading: frequency, 2, 4, 6 Hz; amplitude 140 kN.	DEM model was validated by comparing the settlement under cyclic loading. The load frequency < 15 Hz has few influences on the ballast layer deformation rate, while load frequency > 15 Hz substantially increases the deformation rate.
Full-scale track model	Esen et al., 2022 [180]	Sample:6 × 2.2 × 1.6 m Particle: not-mentioned	Cyclic loading: frequency, 2.5, 5.6 Hz; amplitude 13–58.9, 5–83.4 kN.	Geosynthetic reinforced soil retaining wall system is a good alternative to a conventional railway embankment because it can improve soil stabilisation and take less land.
Full scale track model	Song et al., 2019 [233]	Sample: 1 sleeper Particle: 4.75–76.2 mm	Cyclic loading: frequency, 2 Hz; amplitude 4.4–44 kN.	DEM model was coupled with FEM model. The DEM model was validated by comparing the pressure under the sleeper. Cyclic loadings compact the ballast below the rail seat and loosen ballast at sleeper ends.
Full scale track model	Liu et al., 2017 [161]	Sample: 2.44 × 1.83 × 0.89 m Particle: 19.1–63.5 mm	Cyclic loading: frequency, 1 Hz; amplitude 130 kN.	The DEM model was validated by comparing the ballast particle acceleration using SmartRock. Ballast movement under cyclic loading has two main type: horizontal movement and horizontal rotation.

wall gap. A tension sensor is installed connecting the geogrid and actuator, which is used to measure the tensile force [181].

Discussions

Main findings

For ballast shape and size, there is an opportunity to improve standards related to the ballast at the construction stage, for example, by considering the physical, mechanical and thermal properties of the individual ballast particles. For ballast degradation and fouling, ballast particle degradation and ballast layer degradation have been long-standing problems, and in the field they are difficult to predict. The solution could be more accurate inspection, for example using GPR or inspection train (instrumented trains) [203,204]. Applying geogrid to coal-fouled ballast layers to enhance the stability is a solution for fouled ballast enhancement [176]. Another method is transforming the ballast layer into a slab, see [205–208].

For ballast layer bulk density and porosity, they can be designed depending different geolocations. For example, in some desert railway

lines, wind-blow sands are accumulated in the voids in ballast layer, for which improving the ballast layer resilience is a good solution [209]. Increasing the bulk density of the ballast layer can be done in two ways (increasing ballast density or ballast layer compaction), which can be used for different situations. For example, increasing ballast density can be applied for the high speed railway line with higher strength steel slag as railway ballast. Reducing porosity and increasing ballast layer compaction can be the solution for high haul, such as using dynamic track stabiliser.

For ballast layer dynamics, the current analysis of the dynamic performance of sleeper-ballast uses simplifications of the track structure, such as scaled ballasted track models and cyclic loading instead of complex dynamic loading/impact loading [210]. To prevent the ballasted track from settling too quickly, the vibration frequency of the ballast layer should be controlled not in the range of 20 Hz to 30 Hz. High ballast layer vibration caused by high stiffness of the ballasted track on bridges may be an application for new ballasted track materials, such as rubber chips, Neoballast or composite sleepers [170,207].

Regarding tests on ballast, classic mechanical laboratory tests usually have some deviations from the actual field. However there has been advancement of laboratory test rigs to better simulate field conditions, such as boundary condition [178,211], test rig size [59] and adding more variables (tamping, water, etc.) [23].

Lastly, some important technologies that did not fit with the current paper structure include: automatic ballast sampler [212], PANDA/ Geoendoscopy coupling [213], GPR [140], LiDAR [214] and trial holes [215].

Future research directions

Particle size and particle size distribution: The future research can be using optimised PSD for ballasted track in desert, which can perform self-cleaning of the sand contamination as well as provide sufficient stiffness and resilience, by the inside structure development (voids, contacts, ballast movements, etc.) of ballast layer.

Particle shape: The future research direction can be applying more normalized particle shape (such as more cubic artificial ballast in Fig. 8) for special railway structures to suppress the excess vibration caused by impact loading. Our new ongoing development is to develop meta material of artificial ballast with the function of self-healing (pending patent).

Particle attrition and fouling: The future research direction can be the high-strength artificial circular ballast. The ballast produces less fines and has self-healing function, which also meets the global goal of carbon neutral.

Ballast layer bulk density: The research direction is combining GPR and axle box acceleration to finally evaluate the ballast layer bulk density, not only on the existing line but also for the quality control of track maintenance (tamping, stabilisation, ballast renewal, etc.).

Ballast testing: In the laboratory testing, the cutting-edge technologies can be combined to obtain more physical information of ballast layer, including GPR, LiDAR (or DIC-related technologies), SmartRock, more realistic loading (impact loading), etc.

Conclusions and perspectives

This paper discusses factors influencing ballast mechanical performance, drawing upon previous research in the field. After reviewing and discussing earlier studies, the following conclusions are given.

Particle size and particle size distribution: Ballast particle size and particle size distribution designed should consider transportation type and environmental conditions (latitude, weather, temperature), in order to improve ballast layer performance (longer service life, higher track stability, etc.).

Particle shape: Ballast shape is a promising property that could be more closely controlled. For example, increasing non-cubic particles may help supress ballast layer vibration.

Particle attrition and fouling: The deterioration of ballast particle geometries and build-up of fouling can lead to rapid track settlement, particularly in wet conditions. Promising areas of investigation to prevent this include more evenly distributing the load from sleeper into ballast (e.g. under-sleeper pads), preventing the development of hanging sleepers (e.g. self-correcting sleepers) and reducing ballast particle abrasion (e.g. ballast rubber inclusions).

Ballast layer bulk density: In-field bulk density measurement remains challenging and a reliable technique for this would be a significant development for the rail industry. Currently 3D GPR appears the most promising approach. Regarding methods to increase bulk density, the most reliable technology is the dynamic track stabiliser, however it is underused in practise.

Ballast testing: a wide range of laboratory test methods have been developed to measure ballast properties, however due to the random arrangement of ballast particle, test repeatability can be challenging. The same is true when comparing lab results to field results – it can be difficult to replicate field conditions in a lab setting. Therefore there is scope to adapt advanced laboratory testing technologies so they can also be deployed in the field.

Declaration of Competing Interest

The authors declare that they have no known competing financial interests or personal relationships that could have appeared to influence the work reported in this paper.

Data availability

No data was used for the research described in the article.

Acknowledgements

This work was supported by the National Key Research and Development Program of China under grant 2022YFB2603304, China Postdoctoral Science Foundation (Grants 2021TQ0213), and Guangdong Basic and Applied Basic Research Foundation (Grants 2021A1515110783). This is from work undertaken as part of the IN2ZONE project, which has received funding from the Shift2Rail Joint Undertaking (JU) under grant agreement 101014571 – IP/ITD/CCA – IP3. Support from the UK's Leverhulme trust is also acknowledged (PLP-2016-270).

Appendix A

Table A1 and Table A2

References

[1] Ali Zakeri J, Esmaeili M, Kasraei A, Bakhtiary A. A numerical investigation on the lateral resistance of frictional sleepers in ballasted railway tracks. Proc Inst Mech Eng, Part F: J Rail Rapid Transit 2014;230(2):440–9.
[2] Guo Y, Markine V, Jing G. Review of ballast track tamping: Mechanism, challenges and solutions. Constr Build Mater 2021;300.
[3] Tutumluer E, Qian Y, Hashash YMA, Ghaboussi J, Davis DD. Discrete element modelling of ballasted track deformation behaviour. Int J Rail Transport 2013;1 (1–2):57–73.
[4] Guo Y, Markine V, Song J, Jing G. Ballast degradation: Effect of particle size and shape using Los Angeles Abrasion test and image analysis. Constr Build Mater 2018;169:414–24.
[5] Kolbuszewski J, Frederick M. The significance of particle shape and size on the mechanical behaviour of granular materials. Eur Conf Soil Mech Found Eng 1963: 253–63.
[6] Marachi ND, Chan CK, Seed HB. Evaluation of properties of rockfill materials. J Soil Mech Found Div 1900;97(SM1).
[7] Indraratna B, Ionescu D, Christie H. Shear behavior of railway ballast based on large-scale triaxial tests. J Geotech Geoenviron Eng 1998;124(5):439–49.
[8] Alabbasi Y, Hussein M. Large-scale triaxial and box testing on railroad ballast: a review. SN Appl Sci 2019;1(12).

[9] Guo YL, Markine V, Qiang WL, Zhang H, Jing GQ. Effects of crumb rubber size and percentage on degradation reduction of railway ballast. Constr Build Mater 2019;212:210–24.
[10] Raymond GP, Diyaljee VA. Railroad ballast sizing and grading. J Geotech Eng Div 1979;105(5):676–81.
[11] Janardhanam R, Desai C. Three-dimensional testing and modeling of ballast. J Geotech Eng 1983;109(6):783–96.
[12] Vallerga B, Seed H, Monismith C, Cooper R. Effect of shape, size, and surface roughness of aggregate particles on the strength of granular materials. ASTM International: Road and Paving Materials; 1957.
[13] Le Pen LM, Powrie W, Zervos A, Ahmed S, Aingaran S. Dependence of shape on particle size for a crushed rock railway ballast. Granul Matter 2013;15(6):849–61.
[14] Boler H, Qian Y, Tutumluer E. Influence of Size and Shape Properties of Railroad Ballast on Aggregate Packing: Statistical Analysis. Transport Res Rec: J Transport Res Board 2014;2448:94–104.
[15] Wang B, Martin U, Rapp S. Discrete element modeling of the single-particle crushing test for ballast stones. Comput Geotech 2017;88:61–73.
[16] Xu Y, Yu W, Qie L, Wang H, Ning N. Analysis of influence of ballast shape on abrasion resistance using discrete element method. Constr Build Mater 2021;273.
[17] Kolos A, Konon A, Chistyakov P. Change of Ballast Strength Properties During Particles Abrasive Wear. Procedia Eng 2017;189:908–15.
[18] Bach H, Veit P. Evaluation of attrition tests for railway ballast, na2013.
[19] Dahal B, Mishra D. Discrete Element Modeling of Permanent Deformation Accumulation in Railroad Ballast Considering Particle Breakage. Front Built Environ 2020;5.
[20] Indraratna B, Salim W. Modelling of particle breakage of coarse aggregates incorporating strength and dilatancy, (2002).
[21] de Bono J, Li H, McDowell G. A new abrasive wear model for railway ballast. Soils Found 2020;60(3):714–21.
[22] Esmaeili M, Yousefian K, Nouri R. Vertical load distribution in ballasted railway tracks with steel slag and limestone ballasts. Int J Pavement Eng 2017:1–8.
[23] Nålsund R. Railway ballast characteristics, selection criterion and performance. Department of Civil and Transport Engineering: Norwegian University of Science and Technology, Trondheim; 2014.
[24] Köken E, Özarslan A, Bacak G. An experimental investigation on the durability of railway ballast material by magnesium sulfate soundness. Granul Matter 2018;20 (2).
[25] Koh T, Moon S-W, Jung H, Jeong Y, Pyo SJS. A Feasibility Study on the Application of Basic Oxygen Furnace (BOF). Steel Slag Railway Ballast Mater 2018;10(2):284.
[26] Esmaeili M, Nouri R, Yousefian K. Experimental comparison of the lateral resistance of tracks with steel slag ballast and limestone ballast materials. Proc Inst Mech Eng, Part F: J Rail Rapid Transit 2016;231(2):175–84.
[27] Ajayi O, Le Pen L, Zervos A, Powrie W. Effects of random fibre reinforcement on the density of granular materials, (2014).
[28] Ferellec J-F, McDowell GR. A method to model realistic particle shape and inertia in DEM. Granul Matter 2010;12(5):459–67.
[29] Liu J, Wang P, Liu G, Xiao J, Liu H, Gao T. Influence of a tamping operation on the vibrational characteristics and resistance-evolution law of a ballast bed. Constr Build Mater 2020;239:117879.
[30] Sun QD, Indraratna B, Nimbalkar S. Deformation and Degradation Mechanisms of Railway Ballast under High Frequency Cyclic Loading. J Geotech Geoenviron Eng 2016;142(1):04015056.
[31] Mishra D, Mahmud SN. Effect of Particle Size and Shape Characteristics on Ballast Shear Strength: A Numerical Study Using the Direct Shear Test, 2017 Joint Rail Conference, American Society of Mechanical Engineers, 2017, pp. V001T01A014-V001T01A014.
[32] Liu S, Huang H, Qiu T, Kerchof B. Characterization of Ballast Particle Movement at Mud Spot. J Mater Civil Eng 2018;31(1):04018339.
[33] Vivanco JR, Barbier S, Navarrete M-AB, Breul P. Statistical Analysis of the Influence of Ballast Fouling on Penetrometer and Geoendoscope Data. Adv Transport Geotech. IV2022, pp. 915-930.
[34] Sadeghi J, Tolou Kian AR, Ghiasinejad H, Fallah Moqaddam M, Motevalli S. Effectiveness of geogrid reinforcement in improvement of mechanical behavior of sand-contaminated ballast. Geotext Geomembr 2020.
[35] Qian Y, Mishra D, Tutumluer E, Kazmee HA. Characterization of geogrid reinforced ballast behavior at different levels of degradation through triaxial shear strength test and discrete element modeling. Geotext Geomembr 2015;43 (5):393–402.
[36] Schmidt S, Shah S, Moaveni M, Landry BJ, Tutumluer E, Basye C, et al. Railway Ballast Permeability and Cleaning Considerations. Transport Res Rec: J Transport Res Board 2017;2607:24–32.
[37] Koohmishi M. Drainage potential of degraded railway ballast considering initial gradation and intrusion of external fine materials. Soils Found 2020.
[38] Goodarzi S, Kashani HF, Saeedi A, Oke J, Ho CL. Stochastic analysis for estimating track geometry degradation rates based on GPR and LiDAR data. Constr Build Mater 2023;369.
[39] Gong Y, Qian Y, Fanucci F. Investigation on the drainage condition within the ballast layer based on 3D CFD simulations. Transp Geotech 2023;39.
[40] Zakeri JA, Barati M. Utilizing the track panel displacement method for estimating vertical load effects on the lateral resistance of continuously welded railway track. Proc Inst Mech Eng, Part F: J Rail Rapid Transit 2013;229(3):262–7.
[41] Guo YL, Zong L, Markine V, Wang XY, Jing GQ. Experimental and numerical study on lateral and longitudinal resistance of ballasted track with nailed sleeper. Int J Rail Transport 2021:1–19.
[42] Nobakht S, Zakeri J-A, Safizadeh A. Investigation on longitudinal resistance of the ballasted railway track under vertical load. Constr Build Mater 2022;317.
[43] Akey EK, Jones MW, Ho CL, Rubin AJ. Measuring Railroad Ballast Modulus of Elasticity Using Light Weight Deflectometer. Adv Transport Geotech IV2022, pp. 269–278.
[44] Guo Y, Wang J, Markine V, Jing G. Ballast Mechanical Performance with and without Under Sleeper Pads. KSCE J Civ Eng 2020.
[45] Zarembski AM, Grissom G, Euston T. Use of ballast inspection technology for the prioritization, planning and management of ballast delivery and placement, American Railway Engineering Association Annual Conference, Indianapolis, 2013.
[46] Le Pen L, Bhandari AR, Powrie W. Sleeper End Resistance of Ballasted Railway Tracks. J Geotech Geoenviron Eng 2014;140(5):04014004.
[47] Shi C, Zhao C, Yang Y, Guo Y, Zhang X. Analysis of Railway Ballasted Track Stiffness and Behavior with a Hybrid Discrete-Continuum Approach. Int J Geomech 2021;21(3).
[48] Guo Y, Zhao C, Markine V, Shi C, Jing G, Zhai W. Discrete element modelling of railway ballast performance considering particle shape and rolling resistance. Railway Eng Sci 2020;28(4):382–407.
[49] T.P.M.o. Railways, Railway Ballast, TB/T2140-2008, China Railway Publishing House, Beijing, 2008.
[50] B.s.p.B.E. British Standards Institution, Aggregates for railway ballast, British Standards Institution London, 2013.
[51] Guo Y, Xie J, Fan Z, Markine V, Connoly D, Jing G. Ballast material selection and evaluation means: A review, (2022).
[52] Indraratna B, Salim W. Mechanics of ballasted rail tracks: a geotechnical perspective. CRC Press; 2005.
[53] Selig ET, Roner CJ. Effects of particle characteristics on behavior of granular material. Transport Res Rec (1131) (1987).
[54] Lobo-Guerrero S, Vallejo LE. Discrete element method evaluation of granular crushing under direct shear test conditions. J Geotech Geoenviron Eng 2005;131 (10):1295–300.
[55] Lackenby J, Indraratna B, McDowell G, Christie D. Effect of confining pressure on ballast degradation and deformation under cyclic triaxial loading. Géotechnique 2007;57(6):527–36.
[56] Roenfeldt MA. A study of mechanical degradation of a coarse aggregate subject to repeated loading, (1980).
[57] Indraratna B, Sun Y, Nimbalkar S. Laboratory assessment of the role of particle size distribution on the deformation and degradation of ballast under cyclic loading. J Geotech Geoenviron Eng 2016;142(7):04016016.
[58] Han X. Evaluation of ballast materials based on ballast particle characteristics and functions. Univ Massachusetts Amherst 1998.
[59] Jia W, Markine V, Guo Y, Jing G. Experimental and numerical investigations on the shear behaviour of recycled railway ballast. Constr Build Mater 2019;217: 310–20.
[60] Wang Z, Jing G, Yu Q, Yin H. Analysis of ballast direct shear tests by discrete element method under different normal stress. Measurement 2015;63:17–24.
[61] Bian X, Huang H, Tutumluer E, Gao Y. "Critical particle size" and ballast gradation studied by Discrete Element Modeling. Transp Geotech 2016;6:38–44.
[62] Guo Y, Zhao C, Markine V, Jing G, Zhai W. Calibration for discrete element modelling of railway ballast: A review. Transp Geotech 2020;23:100341.
[63] Guo Y, Markine V, Zhang X, Qiang W, Jing G. Image analysis for morphology, rheology and degradation study of railway ballast: A review. Transp Geotech 2019;18:173–211.
[64] Li D, Hyslip J, Sussmann T, Chrismer S. Railway geotechnics. CRC Press; 2015.
[65] Esmaeili M, Zakeri JA, Ebrahimi H, Khadem Sameni M. Experimental study on dynamic properties of railway ballast mixed with tire derived aggregate by modal shaker test. Adv Mech Eng 2016;8(5).
[66] Dissanayake D, Kurukulasuriya L, Dissanayake P. Evaluation of shear strength parameters of rail track ballast in Sri Lanka. J Natl Sci Found 2016;44(1).
[67] Zhao S, Zhou X, Liu W. Discrete element simulations of direct shear tests with particle angularity effect. Granul Matter 2015;17(6):793–806.
[68] Kodicherla SPK, Gong G, Yang ZX, Krabbenhoft K, Fan L, Moy CKS, et al. The influence of particle elongations on direct shear behaviour of granular materials using DEM. Granul Matter 2019;21(4).
[69] Liu Y, Gao R, Chen J. Exploring the influence of sphericity on the mechanical behaviors of ballast particles subjected to direct shear. Granul Matter 2019;21(4).
[70] Chen J, Gao R, Liu Y. Numerical Study of Particle Morphology Effect on the Angle of Repose for Coarse Assemblies Using DEM. Adv Mater Sci Eng 2019;2019:1–15.
[71] Danesh A, Mirghasemi AA, Palassi M. Evaluation of particle shape on direct shear mechanical behavior of ballast assembly using discrete element method (DEM). Transp Geotech 2020;23.
[72] de Paiva CE, Pereira ML, Ribeiro RP, Santos RS. Evaluation of ballast materials used in Brazilian railways based on their resistance to wear. Proceedings of the International Conference on Road and Rail Infrastructure CETRA. 2018.
[73] Juhász E, Fischer SJPP. Investigation of railroad ballast particle breakage. 2019; 14(2):3–14.
[74] Jing GQ, Ji YM, Qiang WL, Zhang R. Experimental and Numerical Study on Ballast Flakiness and Elongation Index by Direct Shear Test. Int J Geomech 2020; 20(10).
[75] Moaveni M, Qian Y, Boler H, Mishra D, Tutumluer E. Investigation of ballast degradation and fouling trends using image analysis, Proc. 2nd Int. Conf. on Railway Technology: Research, Development and Maintenance (Pombo, J.(ed.)). Stirlingshire, UK: Civil-Comp Press, Paper, 2014.
[76] Sun Y, Zheng C. Breakage and shape analysis of ballast aggregates with different size distributions. Particuology 2017;35:84–92.

[77] Sevi AF. Physical modeling of railroad ballast using the parallel gradation scaling technique within the cyclical triaxial framework. Missouri University of Science and Technology; 2008.
[78] Roner CJ. Some effects of shape, gradation and size on the performance of railroad ballast, M. Sc. Degree project report, Report No. AAR85-324P, Department of Civil Engineering, University of Massachusetts, Amherst, Massachusetts (1985).
[79] A.J.R.E.E.P. Aikawa, Edinburgh, UK, Impact-loading-test regarding ballast subsidence countermeasures using high-damping under sleeper pads and high-strength artificial ballast cubes, (2017).
[80] Bian X, Li W, Qian Y, Tutumluer E. Micromechanical Particle Interactions in Railway Ballast through DEM Simulations of Direct Shear Tests. Int J Geomech 2019;19(5).
[81] Indraratna B, Salim W, Rujikiatkamjorn C. Advanced rail geotechnology: Ballasted track. CRC Press London; 2011.
[82] Wong CPY, Coop MR. The Development of Inter-Particle Friction in a Railway Ballast. Géotechnique Lett 2020;10(4):1–23.
[83] Suhr B, Butcher TA, Lewis R, Six K. Friction and wear in railway ballast stone interfaces. Tribol Int 2020;151.
[84] Raymond GP. Research on railroad ballast specification and evaluation. Transport Res Rec 1985;1006:1–8.
[85] Mvelase GM, Gräbe P, Anochie-Boateng JK. The use of laser technology to investigate the effect of railway ballast roundness on shear strength. Transport Geotech 2017;11:97–106.
[86] Fardin Rosa A, Sacramento Aragão FT, Motta LMGd. Effects of particle size distribution and lithology on the resistance to breakage of ballast materials. Constr Build Mater (2020).
[87] Rohrman AK, Kashani HF, Ho CL. Effects of natural abrasion on railroad ballast strength and deformation properties. Constr Build Mater 2020;247.
[88] Huang H. Discrete element modeling of railroad ballast using imaging based aggregate morphology characterization. University of Illinois at Urbana-Champaign; 2010.
[89] Tutumluer E, Huang H, Hashash Y, Ghaboussi J. Aggregate shape effects on ballast tamping and railroad track lateral stability. AREMA Annual Conference, Loisville, KY, Sept, 2006, p. 17–20.
[90] Thorn N, Brown S. The mechanical properties of unbound aggregates from various sources, Unbound aggregates in roads. Elsevier 1989:130–42.
[91] Thom N, Brown S. The effect of grading and density on the mechanical properties of a crushed dolomitic limestone, Australian Road Research Board (ARRB) Conference, 14th, 1988, Canberra, 1988.
[92] Koohmishi M, Palassi M. Degradation of railway ballast under impact loading considering the morphological properties of aggregate. Transp Geotech 2020;25.
[93] Tew G, Marich S, Mutton JJR. BHP Research-Melbourne Laboratories for Railways of Australia, A review of track design procedures, (1991).
[94] Marsal RJ. Large-scale testing of rockfill materials. J Soil Mech Found Divis 1967;93(2):27–43.
[95] Chrismer S, Selig E. Computer model for ballast maintenance planning. Proceedings of 5th international heavy haul railway conference, beijing, china, 1993, p. 223–7.
[96] Aikawa A. Dynamic characterisation of a ballast layer subject to traffic impact loads using three-dimensional sensing stones and a special sensing sleeper. Constr Build Mater 2015;92:23–30.
[97] Lackenby J. Triaxial behaviour of ballast and the role of confining pressure under cyclic loading, (2006).
[98] Lobo-Guerrero S, Vallejo LE. Discrete Element Method Analysis of Railtrack Ballast Degradation during Cyclic Loading. Granul Matter 2006;8(3–4):195–204.
[99] Raymond GP, Bathurst RJ. Performance of large-scale model single tie-ballast systems, 1987.
[100] Selig ET, Waters JM. Track geotechnology and substructure management. Thomas Telford 1994.
[101] Charoenwong C, Connolly DP, Colaço A, Alves Costa P, Woodward PK, Romero A, et al. Railway slab vs ballasted track: A comparison of track geometry degradation. Constr Build Mater 2023;378.
[102] Sun Q, Indraratna B, Nimbalkar S. Effect of cyclic loading frequency on the permanent deformation and degradation of railway ballast. Géotechnique 2014.
[103] Wnek M, Tutumluer E, Moaveni M, Gehringer E. Investigation of Aggregate Properties Influencing Railroad Ballast Performance. Transport Res Rec: J Transport Res Board 2013;2374:180–9.
[104] Kim J, Park B-S, Woo SI, Choi Y-T. Evaluation of ballasted-track condition based on aggregate-shape characterization. Constr Build Mater 2020;232.
[105] Zhang Z-T, Gao W-H, Wang X, Zhang J-Q, Tang X-Y. Degradation-induced evolution of particle roundness and its effect on the shear behaviour of railway ballast. Transport Geotech 2020;24.
[106] McDowell GR, Humphreys A. Yielding of granular materials. Granul Matter 2014;4(1):1–8.
[107] Bolton M, Nakata Y, Cheng Y. Micro-and macro-mechanical behaviour of DEM crushable materials. Géotechnique 2008;58(6):471–80.
[108] Cheng Y, Nakata Y, Bolton M. Discrete element simulation of crushable soil. Geotechnique 2003;53(7):633–41.
[109] McDowell G, Amon A. The application of Weibull statistics to the fracture of soil particles. Soils Found 2000;40(5):133–41.
[110] Liu Z, Feng B, Tutumluer E. Effect of Ballast Degradation on Track Dynamic Behavior Using Discrete Element Modeling. Transport Res Rec: J Transport Res Board 2022.
[111] Gong Y, Qian Y, Chen X. Comparison of Ballast Drainage Improvement Between Track Lifting and Shoulder Cleaning Based on CFD Simulations. Transport Res Rec: J Transport Res Board 2022.
[112] Chawla S, Shahu JT. Reinforcement and mud-pumping benefits of geosynthetics in railway tracks: Model tests. Geotext Geomembr 2016;44(3):366–80.
[113] Tennakoon N, Indraratna B, Rujikiatkamjorn C, Nimbalkar S, Neville T. The Role of Ballast-Fouling Characteristics on the Drainage Capacity of Rail Substructure. Geotech Test J 2012;35(4).
[114] Huang H, Tutumluer E. Discrete Element Modeling for fouled railroad ballast. Constr Build Mater 2011;25(8):3306–12.
[115] Wu C. Research on tamping mechanism of harden railway roadbed. Sourthwest Jiaotong University 2016.
[116] Liu J, Liu Z, Wang P, Kou L, Sysyn M. Dynamic characteristics of the railway ballast bed under water-rich and low-temperature environments. Eng Struct 2022;252.
[117] N.R.o.P.s.R.o. China, Rules for Maintenance of Ballasted Track on High Speed Railway: TG/GW 116-2013, China Railway Publishing House, Beijing, 2013.
[118] W.L. Lim, Mechanics of railway ballast behaviour, University of Nottingham, 2004.
[119] E.T. Selig, Ballast for heavy duty track, TRACK TECHNOLOGY, pp. 245-252.
[120] Sadeghi J, Tolou Kian AR, Chopani M, Khanmoradi A. Effects of particle gradations on cyclic behavior of ballast contaminated with sand. Constr Build Mater 2022;342.
[121] Ebrahimi A, Tinjum JM, Edil TB. Deformational behavior of fouled railway ballast. Can Geotech J 2015;52(3):344–55.
[122] Huang H, Tutumluer E, Dombrow W. Laboratory characterization of fouled railroad ballast behavior. Transport Res Rec: J Transport Res Board 2009;2117:93–101.
[123] Indraratna B, Ionescu D, Christie D, Chowdhury R. Compression and degradation of railway ballast under one-dimensional loading, (1997).
[124] Indraratna B, Ngo NT, Rujikiatkamjorn C, Vinod J. Behavior of fresh and fouled railway ballast subjected to direct shear testing: discrete element simulation. Int J Geomech 2012;14(1):34–44.
[125] Chen J, Gao R, Liu Y, Shi Z, Zhang R. Numerical exploration of the behavior of coal-fouled ballast subjected to direct shear test. Constr Build Mater 2021;273.
[126] Paiva C, Ferreira M, Ferreira A. Ballast drainage in Brazilian railway infrastructures. Constr Build Mater 2015;92:58–63.
[127] Huang H, Moaveni M, Schmidt S, Tutumluer E, Hart JM. Evaluation of Railway Ballast Permeability Using Machine Vision-Based Degradation Analysis. Transp Res Rec 2018;0361198118790849.
[128] Liu J, Wang P, Liu G, Dai J, Xiao J, Liu H. Study of the characteristics of ballast bed resistance for different temperature and humidity conditions. Constr Build Mater 2021;266.
[129] Nurmikolu A. Fouling and frost susceptibility of railway ballast and subballast, field and laboratory study, 2010.
[130] Terzaghi K, Peck RB, Mesri G. Soil mechanics in engineering practice. John Wiley & Sons; 1996.
[131] K.H. Roscoe, A. Schofield, a.P.J.G. Wroth, On the yielding of soils, 8(1) (1958) 22–53.
[132] Schofield AN, Wroth P. Critical state soil mechanics. McGraw-hill London 1968.
[133] P.N. Gaskin, A.G. Powell, G.J.T.E.J.o.A. Raymond, Response of railroad ballast to vertical vibration, 104(1) (1978) 75–87.
[134] Aursudkij B. A laboratory study of railway ballast behaviour under traffic loading and tamping maintenance, University of Nottingham, 2007.
[135] Monismith CL, Hicks RG, Salam Y. Basic properties of pavement components, 1971.
[136] Kolisoja P. Resilient deformation characteristics of granular materials, Tampere University of Technology Finland, Publications1997.
[137] Indraratna B, Ionescu D. State of the art large scale testing of ballast, (2000).
[138] Shenton MJSMS. British Railways Research Departement, Derby, England, Deformation of railway ballast under repeated loading triaxial tests, (1974).
[139] O'Reilly MP, Brown SF. Cyclic loading of soils: from theory to design, Blackie Glasgow, UK1991.
[140] Guo Y, Wang S, Jing G, Liu G. State-of-art review of Ground Penetration Radar (GPR) application on railway ballast inspection, (2022).
[141] Guo Y, Wang S, Jing G, Yang F, Liu G, Qiang W, Wang Y. Assessment of ballast layer under multiple field conditions in China, (2022).
[142] Guo Y, Liu G, Jing G, Qu J, Wang S, Qiang W. Ballast fouling inspection and quantification with ground penetrating radar (GPR). Int J Rail Transport 2022:1–18.
[143] Jing G, Ding D, Liu X. High-speed railway ballast flight mechanism analysis and risk management – A literature review. Constr Build Mater 2019;223:629–42.
[144] Lichtberger B. Track Compendium: Formation, Permanent Way, Maintenance. Economics 2005;1.
[145] Esmaeili M, Siahkouhi M. Tire-derived aggregate layer performance in railway bridges as a novel impact absorber: Numerical and field study. Struct Control Health Monit 2019.
[146] Rebelo C, Simões da Silva L, Rigueiro C, Pircher M. Dynamic behaviour of twin single-span ballasted railway viaducts — Field measurements and modal identification. Eng Struct 2008;30(9):2460–9.
[147] Mohammadzadeh S, Miri A, Nouri M. Enhancing the Structural Performance of Masonry Arch Bridges with Ballast Mats. J Perform Constr Facil 2017;31(5).
[148] Aela P, Jia WL, Jing GQ. Effect of ballast retaining walls on the lateral resistance of railway tracks. Proc Inst Mech Eng, Part F: J Rail Rapid Transit 2020;235(4):416–24.

[149] Sysyn M, Kovalchuk V, Gerber U, Nabochenko O, Pentsak A. Experimental study of railway ballast consolidation inhomogeneity under vibration loading. Pollack Periodica 2020;15(1):27–36.
[150] Causse J, Pison F, Simon C, Coudert F, Pouligny P. Influence of the distance between bridge and expansion joint on the track geometry measurement for high-speed railway lines. Railway Eng Conf 2015.
[151] Zhai W, Han Z, Chen Z, Ling L, Zhu S. Train–track–bridge dynamic interaction: a state-of-the-art review. Veh Syst Dyn 2019;57(7):984–1027.
[152] Alexakis H, Franza A, Acikgoz S, DeJong M. A multi-sensing monitoring system to study deterioration of a railway bridge, (2019).
[153] Yan B, Dai G-L, Zhang H-P. Beam-track interaction of high-speed railway bridge with ballast track. J Cent South Univ 2012;19(5):1447–53.
[154] Cheng Y, Au F, Cheung Y. Vibration of railway bridges under a moving train by using bridge-track-vehicle element. Eng Struct 2001;23(12):1597–606.
[155] Mohammadzadeh S, Miri A. Ballast Cleaning as a Solution for Controlling Increased Bridge Vibrations due to Higher Operational Speeds. J Perform Constr Facil 2018;32(5):04018064.
[156] Gao L, Luo Q, Xu Y, Jing G-Q, Jiang H-K. Discrete element method of improved performance of railway ballast bed using elastic sleeper. J Cent South Univ 2015;22(8):3223–31.
[157] Luo Q. Research of High speed Railway Ballast Mechanics Based on Discrete Element Method. Beijing: Beijing Jiaotong University; 2014.
[158] Liu H, Xiao J, Wang P, Liu G, Gao M, Li S. Experimental investigation of the characteristics of a granular ballast bed under cyclic longitudinal loading. Constr Build Mater 2018;163:214–24.
[159] Nakamura T, Momoya Y, Nomura K, Yoshihiko Y. Shaking Table Test Using Full-scale Model for Lateral Resistance Force of Ballasted Tracks During Earthquake. Procedia Eng 2016;143:1100–7.
[160] Chen R, Wei X, Wang P, Liu H, Xiao J, Xu J. Shaking table testing and numerical modeling of continuous welded ballast track on bridges under longitudinal seismic loading. J Vibroeng 2017;19(5):3610–28.
[161] Liu S, Huang H, Qiu T, Gao L. Comparison of Laboratory Testing Using SmartRock and Discrete Element Modeling of Ballast Particle Movement. J Mater Civil Eng 2017;29(3):D6016001.
[162] Fu L, Tian Z, Zhou S, Zheng Y, Wang B. Characterization of ballast particle's movement associated with loading cycle, magnitude and frequency using SmartRock sensors. Granul Matter 2020;22(3).
[163] Zeng K, Qiu T, Bian XC, Xiao M, Huang H. Identification of ballast condition using SmartRock and pattern recognition. Constr Build Mater 2019;221:50–9.
[164] Zhang X, Zhao C, Zhai W. Dynamic Behavior Analysis of High-Speed Railway Ballast under Moving Vehicle Loads Using Discrete Element Method. Int J Geomech 2016;17(7):04016157.
[165] Guo Y, Shi C, Zhao C, Markine V, Jing G. Numerical analysis of train-track-subgrade dynamic performance with crumb rubber in ballast layer. Constr Build Mater 2022;336.
[166] Liu G, Cong J, Wang P, Du S, Wang L, Chen R. Study on vertical vibration and transmission characteristics of railway ballast using impact hammer test. Constr Build Mater 2022;316.
[167] Zhai W, Wang K, Lin J. Modelling and experiment of railway ballast vibrations. J Sound Vib 2004;270(4):673–83.
[168] Ji S, Liu L. DEM Analysis of Mechanical Behaviors of Railway Ballast. In: Computational Granular Mechanics and Its Engineering Applications. Springer; 2020. p. 311–58.
[169] Xiao J-L, Liu G-Z, Liu J-X, Dai J-C, Liu H, Wang P. Parameters of a discrete element ballasted bed model based on a response surface method. J Zhejiang Univ-Sci A 2019;20(9):685–700.
[170] Guo Y, Ji Y, Zhou Q, Markine V, Jing G. Discrete Element Modelling of Rubber-Protected Ballast Performance Subjected to Direct Shear Test and Cyclic Loading. Sustainability 2020;12(7).
[171] Jing GQ, Qie LC, Markine V, Jia WL. Polyurethane reinforced ballasted track: Review, innovation and challenge. Constr Build Mater 2019;208:734–48.
[172] Ho C, Humphrey D, Hyslip J, Moorhead W. Use of Recycled Tire Rubber to Modify Track-Substructure Interaction. Transport Res Rec: J Transport Res Board 2013;2374:119–25.
[173] Qian Y, Boler H, Moaveni M, Tutumluer E, Hashash YM, Ghaboussi J. Degradation-Related Changes in Ballast Gradation and Aggregate Particle Morphology. J Geotech Geoenviron Eng 2017;143(8):04017032.
[174] Zhao H, Chen J, Giorgio I. A Numerical Study of Railway Ballast Subjected to Direct Shearing Using the Discrete Element Method. Adv Mater Sci Eng 2020;2020:1–13.
[175] Liu J, Wang P, Liu G, Zhang M, Xiao J, Liu H. Uniaxial compression characteristics of railway ballast combined with ice. Constr Build Mater 2020;263.
[176] Ngo NT, Indraratna B, Rujikiatkamjorn C. DEM simulation of the behaviour of geogrid stabilised ballast fouled with coal. Comput Geotech 2014;55:224–31.
[177] Xiao J, Zhang D, Wei K, Luo Z. Shakedown behaviors of railway ballast under cyclic loading. Constr Build Mater 2017;155:1206–14.
[178] Yu Z, Connolly DP, Woodward PK, Laghrouche O, Tutumluer E. Railway ballast anisotropy testing via true triaxial apparatus. Transport Geotech 2020;23.
[180] Esen AF, Woodward PK, Laghrouche O, Connolly DP. Stress distribution in reinforced railway structures. Transport Geotech 2022;32.
[181] Chen C, McDowell GR, Thom NH. Investigating geogrid-reinforced ballast: Experimental pull-out tests and discrete element modelling. Soils Found 2014;54(1):1–11.
[182] Nålsund R. Effect of Grading on Degradation of Crushed-Rock Railway Ballast and on Permanent Axial Deformation. Transport Res Rec: J Transport Res Board 2010;2154:149–55.
[183] Qian Y, Tutumluer E, Hashash YMA, Ghaboussi J. Effects of Ballast Degradation on Permanent Deformation Behavior From Large-Scale Triaxial Tests, (2014) V001T01A022.
[184] Ngo NT, Indraratna B, Rujikiatkamjorn C. Micromechanics-Based Investigation of Fouled Ballast Using Large-Scale Triaxial Tests and Discrete Element Modeling. J Geotech Geoenviron Eng 2017;143(2).
[185] Kashani HF, Ho CL, Hyslip JP. Fouling and water content influence on the ballast deformation properties. Constr Build Mater 2018;190:881–95.
[186] Qian Y, Tutumluer E, Mishra D, Kazmee H. Triaxial testing and discrete-element modelling of geogrid-stabilised rail ballast. Proc Inst Civil Eng - Ground Improvement 2018;171(4):223–31.
[187] Mishra D, Qian Y, Kazmee H, Tutumluer E. Investigation of Geogrid-Reinforced Railroad Ballast Behavior Using Large-Scale Triaxial Testing and Discrete Element Modeling. Transport Res Rec: J Transport Res Board 2014;2462:98–108.
[188] Menan Hasnayn M, John McCarter W, Woodward PK, Connolly DP, Starrs G. Railway subgrade performance during flooding and the post-flooding (recovery) period. Transport Geotech 2017;11:57–68.
[189] Hasnayn MM, McCarter WJ, Woodward PK, Connolly DP. Railway subgrade performance after repeated flooding – Large-scale laboratory testing. Transport Geotech 2020;23.
[190] Abadi T, Le Pen L, Zervos A, Powrie W. A review and evaluation of ballast settlement models using results from the Southampton Railway Testing Facility (SRTF). Procedia Eng 2016;143:999–1006.
[191] Sol-Sánchez M, Moreno-Navarro F, Rubio-Gámez M, Manzo N, Fontseré V. Full-scale study of Neoballast section for its application in railway tracks: optimization of track design. Mater Struct 2018;51(2):43.
[192] Aursudkij B, McDowell GR, Collop AC. Cyclic loading of railway ballast under triaxial conditions and in a railway test facility. Granul Matter 2009;11(6):391–401.
[193] Indraratna B, Ngo T. Ballast railroad design: smart-uow approach. CRC Press; 2018.
[194] Li W, Bian X, Duan X, Tutumluer E. Full-Scale Model Testing on Ballasted High-Speed Railway: Dynamic Responses and Accumulated Settlements. Transport Res Rec: J Transport Res Board 2018;2672(10):125–35.
[195] Gu Q, Liu H, Wu Y, Luo Z, Bian X. Evolution of trackbed performance and ballast degradation due to passages of million train wheel axle loads. Transport Geotech 2022;34.
[196] Ramos A, Gomes Correia A, Calçada R, Alves Costa P, Esen A, Woodward PK, et al. Influence of track foundation on the performance of ballast and concrete slab tracks under cyclic loading: Physical modelling and numerical model calibration. Constr Build Mater 2021;277.
[197] Qiu M-M, Yang G-L, Shen Q, Yang X, Wang G, Lin Y-L. Dynamic behavior of new cutting subgrade structure of expensive soil under train loads coupling with service environment. J Cent South Univ 2017;24(4):875–90.
[198] Indraratna B, Ngo T, Bessa Ferreira F, Rujikiatkamjorn C, Tucho A. Large-scale Testing Facility for Heavy Haul Track. Transport Geotech 2021.
[199] Estaire J, Cuéllar V, Santana M. Testing railway tracks at 1: 1 scale at CEDEX Track Box. Proceedings of the Intern. Cong. on High-Speed Rail. Technologies and Long Term Impacts (2017).
[200] Jing GQ, Aela P. Review of the lateral resistance of ballasted tracks. P I Mech Eng F-J Rai 2020;234(8):807–20.
[201] Ling X, Xiao H, Jin F. Investigating the effect of different bonding areas on the lateral resistance of polyurethane-mixed ballast using the discrete element method. Proc Inst Mech Eng, Part F: J Rail Rapid Transit 2020.
[202] Ichikawa T, Hayano K, Nakamura T, Momoya Y. Lateral resistance of ballasted tracks for various shapes of sleepers based on limit equilibrium methods. Japan Geotech Soc Spec Publ 2016;2(46):1632–5.
[203] Guo Y, Wang S, Jing G, Liu G. Ballast fouling inspection and quantification with Ground Penetrating Radar (GPR), (2022).
[204] Zhao W, Qiang W, Yang F, Jing G, Guo Y. Ballast layer defect inspection using data analysis of track irregularity.
[205] Esmaeili M, Paricheh M, Esfahani MH. Laboratory investigation on the behavior of ballast stabilized with bitumen-cement mortar. Constr Build Mater 2020;245:118389.
[206] Lee I-W, Pyo S, Jung Y-H. Development of quick-hardening infilling materials for composite railroad tracks to strengthen existing ballasted track. Compos B Eng 2016;92:37–45.
[207] Esmaeili M, Namaei P. Effect of mother rock strength on rubber-coated ballast (RCB) deterioration. Constr Build Mater 2022;316.
[208] Lee S, Jang SY, Kim CY, Ahn EJ, Kim SP, Gwon S, et al. Effects of Redispersible Polymer Powder on Mechanical and Durability Properties of Preplaced Aggregate Concrete with Recycled Railway Ballast. Int J Concr Struct Mater 2018;12(1).
[209] Esmaeili M, Aela P, Hosseini A. Experimental assessment of cyclic behavior of sand-fouled ballast mixed with tire derived aggregates. Soil Dyn Earthq Eng 2017;98:1–11.
[210] Liu X. Development of Condition Monitoring System for Railway Crossings: Condition Assessment and Degradation Detection for Guided Maintenance, (2020).
[211] Chen C, Indraratna B, McDowell G, Rujikiatkamjorn C. Discrete element modelling of lateral displacement of a granular assembly under cyclic loading. Comput Geotech 2015;69:474–84.
[212] Lim W, Brough M, Middleton SJSWPEC. Prediction of ballast return from high output ballast cleaners (HOBC), (2010).
[213] Haddani Y, Breul P, Saussine G, Navarrete MAB, Ranvier F, Gourvès R. Trackbed Mechanical and Physical Characterization using PANDA®/Geoendoscopy Coupling. Procedia Eng 2016;143:1201–9.

[214] Sadeghi J, Najar MEM, Zakeri JA, Kuttelwascher C. Development of railway ballast geometry index using automated measurement system. Measurement 2019;138:132–42.
[215] Mishra D, Tutumluer E, Stark TD, Hyslip JP, Chrismer SM, Tomas M. Investigation of differential movement at railroad bridge approaches through geotechnical instrumentation. J Zheijang Univ Sci A 2012;13(11):814–24.
[216] Fu J-J, Chen C, Ferellec J-F, Yang J. Effect of Particle Shape on Repose Angle Based on Hopper Flow Test and Discrete Element Method. Adv Civil Eng 2020; 2020:1–10.
[217] Suhr B, Marschnig S, Six K. Comparison of two different types of railway ballast in compression and direct shear tests: experimental results and DEM model validation. Granul Matter 2018;20(4):70.
[218] Gong H, Song W, Huang B, Shu X, Han B, Wu H, et al. Direct shear properties of railway ballast mixed with tire derived aggregates: Experimental and numerical investigations. Constr Build Mater 2019;200:465–73.
[219] Ngo NT, Indraratna B, Rujikiatkamjorn C. Modelling geogrid-reinforced railway ballast using the discrete element method. Transp Geotech 2016;8:86–102.
[220] Harkness J, Zervos A, Le Pen L, Aingaran S, Powrie W. Discrete element simulation of railway ballast: modelling cell pressure effects in triaxial tests. Granul Matter 2016;18(3):1–13.
[221] Liu S, Qiu T, Qian Y, Huang H, Tutumluer E, Shen S. Simulations of large-scale triaxial shear tests on ballast aggregates using sensing mechanism and real-time (SMART) computing. Comput Geotech 2019;110:184–98.
[222] Ngo T, Indraratna B. Analysis of Deformation and Degradation of Fouled Ballast: Experimental Testing and DEM Modeling. Int J Geomech 2020;20(9).
[223] Qian Y, Lee SJ, Tutumluer E, Hashash YMA, Ghaboussi J. Role of Initial Particle Arrangement in Ballast Mechanical Behavior. Int J Geomech 2018;18(3): 04017158.
[224] Indraratna B, Ngo T, Rujikiatkamjorn C. Performance of Ballast Influenced by Deformation and Degradation: Laboratory Testing and Numerical Modeling. Int J Geomech 2019;20(1):04019138.
[225] Indraratna B, Thakur PK, Vinod JS. Experimental and numerical study of railway ballast behavior under cyclic loading. Int J Geomech 2009;10(4):136–44.
[226] Laryea S, Safari Baghsorkhi M, Ferellec JF, McDowell GR, Chen C. Comparison of performance of concrete and steel sleepers using experimental and discrete element methods. Transport Geotech 2014;1(4):225–40.
[227] Xiao J, Zhang D, Zhang X. Effect of Irregular Shape and Cyclic Loading Frequency on the Dynamic Behavior of Railway Ballast. Adv Environ Vib Transport Geodynam 2020:563–75.
[228] Feng B, Park EH, Huang H, Li W, Tutumluer E, Hashash YMA, et al. Discrete Element Modeling of Full-Scale Ballasted Track Dynamic Responses from an Innovative High-Speed Rail Testing Facility. Transport Res Rec: J Transport Res Board 2019.
[229] Khatibi F, Esmaeili M, Mohammadzadeh S. DEM analysis of railway track lateral resistance. Soils Found 2017;57(4):587–602.
[230] Esmaeili M, Majidi-Parast S, Hosseini A. Comparison of dynamic lateral resistance of railway concrete, wooden and steel sleepers subjected to impact loading. Road Mater Pavement Des 2018:1–28.
[231] Li L, Liu W, Ma M, Jing G, Liu W. Research on the dynamic behaviour of the railway ballast assembly subject to the low loading condition based on a tridimensional DEM-FDM coupled approach. Constr Build Mater 2019;218: 135–49.
[232] Zhang X, Zhao C, Zhai W. Importance of load frequency in applying cyclic loads to investigate ballast deformation under high-speed train loads. Soil Dyn Earthq Eng 2019;120:28–38.
[233] Song W, Huang B, Shu X, Stránský J, Wu H. Interaction between Railroad Ballast and Sleeper: A DEM-FEM Approach. Int J Geomech 2019;19(5):04019030.

Further reading

[179] Indraratna B, Ngo NT, Rujikiatkamjorn C. Improved performance of ballasted rail tracks using plastics and rubber inclusions. Procedia Eng 2017;189:207–14.